A reference formulation for computing mass transfer rates of multi-component droplets undergoing general phase-change

Artur Carvalho Santos[a,*], Fernando Luiz Sacomano Filho[b], Aymeric Vié[a,c]

[a]*Laboratoire EM2C, CNRS, CentraleSupélec, Université Paris-Saclay, Gif-sur-Yvette, France.*

[b]*Laboratory of Environmental and Thermal Engineering, Universidade de São Paulo, São Paulo, Brazil.*

[c]*Fédération de Mathématiques, CentraleSupélec, Université Paris-Saclay, Gif-sur-Yvette, France.*

Abstract

Mass diffusion is one of the key physical mechanisms inherent to the phase change of multi-component droplets. Modeling strategies often rely on simplifying assumptions such as Fick's law or the Hirschfelder and Curtiss' approximation. This work seeks to propose a droplet mass transfer formulation based on the Stefan-Maxwell equations without simplifying assumptions for diffusion closures. Such an option has already been investigated by Tonini and Cossali (Int. J. Heat and Mass Transfer, 2016). However, critical simplifications were employed in the analytical developments. In this work, we relax these simplifications with a final model that handles any number of species in general phase-change scenarios (evaporation and/or condensation), applicable to convective environments, and with no hypotheses for the diffusion coefficients' structure, such that it can be regarded as a reference. To show the impact of diffusion simplifications, this formulation is compared with two other approaches representing most mass transfer models used by the literature. In particular, the model originally proposed by Law (Combust. and Flame, 1976) is detailed here since its core results are still among the most used. The proposed formulation is validated with experimental data, and simulations are conducted for droplets of multiple fuel compositions with fixed or varying conditions at the far-away state to map diverse scenarios.

Keywords: Droplet evaporation, Multi-component droplets, Droplet mass transfer, Evaporation modeling, Spray combustion

1. Introduction

Droplet phase change modeling plays a key role in a wide range of applications. For instance, it controls the fuel availability in spray combustion [1]. For this type of application, it is, therefore, crucial for modeling strategies to be able to capture the most physics to reproduce accurate flame structures since this will, in turn, lead to better combustion chamber design.

To this merit, we recently demonstrated the generality of an energy formulation [2] to provide heat transfer rates for multi-component droplets undergoing phase change so that it can be coupled with most mass transfer strategies. Care was taken such that the model was derived to still include more complex physics, such as enthalpy diffusion effects, with no additional structural complexities. For the mass transfer counterpart, however, there is no clear consensus currently, with a substantial number of strategies existing in the literature.

Among the first published works on the treatment of multi-component droplet evaporation is the contribution of Wood et al. [3]. Even though the theoretical development is lacking, the authors published an expression that retrieves the global mass transfer rate of a droplet composed of two components. This was further developed in [4] where the author shows that Wood et al.'s main result corresponds to an evaporation rate constant used in a classical $\mathcal{D}^2$ evaporation law. As a first result, the contribution of Wood et al. [3] is useful, providing a structure that could be expanded to accommodate more species.

However, one of the main features that we highlight is the ability of a multi-component phase-change model to provide expressions for the mass transfer rates of each participating species, not only the global mass transfer rate. This is a key characteristic of a discrete component model (DCM), also referred to as a discrete multi-component [5, 6]. Within this category, one of the most used approaches today dates back to the work of Law [7], where a theoretical framework is developed to study spherical laminar diffusion flames that completely surround a droplet. Among the showcased results, expressions for the fractional evaporation rates, the contribution to the total

*Corresponding author
Email address: artur.carvalho-santos@centralesupelec.fr (Artur Carvalho Santos)

evaporation rate from each species, are provided. As shown in the present work, the main characteristic of Law's model is the assumption of equal diffusion coefficients between all species in the gaseous phase. Therein, although no differential diffusion is accounted for, preferential diffusion occurs as non-unity Lewis numbers are allowed. This is a useful simplification that creates an analytical structure analogous to classical single-component droplet treatments. However, this can be regarded as contradictory: DCMs seek to provide distinguished contributions from each species, so it would be best if the diffusional behavior of each species could also be described separately since diffusion is one of the main mechanisms of mass transfer. Still, it should be noted that other strategies are in development in the literature. One point of contention against DCMs, for example, is that they usually employ the assumption of infinite liquid diffusivity inside the droplet, i.e., the mass fractions of each individual species are uniform inside the droplet and equal to the one at its surface. This, of course, is usually done to avoid having to solve the species diffusion equation inside the droplet and thus reduce computational costs. This has been brought to attention, for instance, in [8], where the author proposes models with different sets of simplifications to try and address this issue.

A natural second approach is, therefore, to relax the hypothesis of equal diffusion coefficients and let each species now have its own average diffusion coefficient; this family of models is here classified through the term differential diffusion. This strategy has been gaining momentum recently, as demonstrated by the useful contributions in the literature, e.g., [9, 10, 11, 12, 13]. In particular, in [13], we proposed a robust numerical strategy with a rigorous analytical treatment that organically incorporates convection and Stefan flow effects for any number of species and for general phase-change conditions.

In this work, we then provide an even finer model, one that does not need any structural hypotheses for diffusion coefficients in the gaseous phase. In this sense, it can be seen as a reference concerning the diffusion treatment, which is paramount for mass transfer strategies. Similar to our previous works, care has been taken such that the final expression can be used for general phase-change (evaporation and/or condensation regimes for each species) with organic incorporation of convection and Stefan flow and no limitations concerning the number and/or type of

liquid or gaseous species. To accomplish this, we depart from general conservation equations for mass and species as well as a general closure for mass diffusion obtained from kinetic theory. We employ usual simplifications to finally analytically integrate the Stefan-Maxwell equations while using results from species conservation, ensuring a coherent model. In particular, this work limits itself to spherical droplets. This is a common strategy that has been used throughout most droplet heat and mass transfer models, which allows for an analytical integration of both the conservation equations and the Stefan-Maxwell equations in a single radial coordinate, as shown in the next section. However, in complex flows, this hypothesis is not straightforward. For instance, in [14], the authors argued that concomitant effects of surface tension and viscous stresses often generate droplet shapes that deviate from the sphere. In this way, the authors from [14] proposed a multi-component droplet mass transfer analytical expression that expands results to spheroidal shapes. Also, in line with typical applications, we neglect the influence of the gravitational force, focusing on small droplets; it is known that for big enough droplets, gravitational effects can also lead to deviations from the sphericity hypothesis and impact key metrics for overall transfer rates onto the surrounding gaseous medium [15] [16].

Of note is the fact that a previous model that analytically integrates the Stefan-Maxwell equations has already been developed in [12]. However, to achieve that model, several restrictions have been imposed. For instance, the analytical development was carried out allowing only a single inert species in the gaseous phase; this could be particularly limiting in gases where many different components can be present surrounding the droplets, as in the case of an atmosphere composed of multiple combustion products, for instance, [17]. Furthermore, as presented, the model is limited to non-convective applications, which can be particularly restraining for the aforementioned spray configurations. Finally, the main strength that we seek to demonstrate, the absence of a structural hypothesis for the diffusion, is also disrupted, since in [12] an additional condition for binary diffusion coefficients between each fuel vapor and the sole inert species is enforced to reach the final result. Therefore, we aim to demonstrate that our final result should enlarge the scope of the original contribution of [12] with no drawbacks. Similarly, since this contribution seeks to extend the results of [12], one perspective would be to consider spheroidal shapes as done in [14], to obtain

a more general model. The relaxation of one degree of freedom concerning the mass diffusion could also be useful when conducting sensitivity analyses for droplet phase-change models, and so this is another advantage of the proposed model. For instance, in [18], the authors conducted an uncertainty quantification study for parameters used in sub-models that affect droplet mass transfer, including binary diffusion coefficients. With the approach proposed here, only binary diffusion coefficients are used to describe the gaseous diffusion, even though a DCM is proposed, which offers more detail for the phase-change description.

This paper is organized as follows. First, we present the analytical derivation of our proposed model, departing from general conservation equations and enforcing hypotheses that are common to all compared mass transfer strategies. Once the final result is obtained, we contrast the main structural differences with regard to the similar strategy developed by Tonini and Cossali [12]. Then, a thorough derivation procedure is also carried out for the foundational model of Law [7]. Indeed, understanding the intricacies of this strategy is still warranted, given that researchers from numerical, theoretical and experimental fronts in the literature have been steadily using its core results for a wide array of applications, see for instance [19, 20, 21, 22, 23, 24, 25, 26, 27, 28, 29, 30]. Therefore, one of the main objectives of this work is to raise awareness that more general strategies exist, in particular the reference we propose that reduces the degrees of freedom for the diffusion description. A third model [13] is then brought to comparison to represent an intermediary diffusion description between the proposed reference and Law's simplified strategy. All mass transfer models are coupled with the general energy formulation previously developed in [2]. Finally, we compare the proposed reference approach with the two simplified DCMs through simulations for droplets composed of different species, describing a gradient of complexity. We first study simple cases where conditions at the far-away state are fixed throughout the droplet's lifetime. Then, as done in [2], we expose droplets to more complex scenarios where the velocity, composition, and temperature at the far-away state are left free to vary following an analytical profile generated through theoretical one-dimensional premixed laminar flames to represent the model application on more general scenarios.

2. Obtaining the reference model: Integration of the Stefan-Maxwell equations

The gas-phase conservation equations for global mass and for an individual species i can be written as follows [31]:

$$\frac{\partial \rho}{\partial t} + \nabla \cdot [\rho \mathbf{u}] = 0, \tag{1}$$

$$\frac{\partial \rho Y_i}{\partial t} + \nabla \cdot [\rho Y_i \mathbf{v}_i^m] = \dot{\omega}_i, \tag{2}$$

where ρ is the density, $\mathbf{u}$ the velocity, Y_i the mass fraction, $\mathbf{v}_i^m$ the average molecular velocity, and $\dot{\omega}_i$ the species source term for chemical reactions.

To simplify the above equations, the following assumptions can be made, as customary in the literature:

2.1. Quasi-steadiness i.e. $\partial/\partial t = 0$;

2.2. Spherical symmetry i.e. $\nabla \cdot \boldsymbol{\gamma} = \frac{d}{dr}[r^2 \boldsymbol{\gamma}]$ for any $\boldsymbol{\gamma}$ (only the radial dimension r is retained);

2.3. No chemical reaction i.e. $\dot{\omega}_k = 0 \ \forall k$.

For the quasi-steadiness hypothesis to be valid, it is essentially assumed that the time scales for processes in the gaseous phase are small compared to the time scale of the evolution of the droplet's radius [32]. In some cases, this can be relaxed, for example, in [33]. As discussed in the introduction, the spherical symmetry is also enforced for simplicity and also to compare and extend results of most currently used droplet phase-change models, which require this hypothesis. As for the absence of chemical reaction, it is assumed that any reactions (including the eventual combustion of evaporated fuels) occur sufficiently far away from the droplet, therefore not affecting its boundary layer development. More details on this hypothesis can be found, for example, in [1] and [34]; again, this same assumption is made for most evaporation models in the literature. For a counter-example, spherical diffusion flames have been studied, for instance, in [7], where the evaporated fuel immediately feeds into a diffusion flame surrounding the droplet.

Applying these hypotheses to Eqs. 1 and 2 leads to:

$$\frac{d}{dr}\left[r^2\rho \mathrm{u}\right] = 0, \tag{3}$$

$$\frac{d}{dr}\left[r^2\rho Y_i \mathrm{v}_i^m\right] = 0. \tag{4}$$

Now, it is possible to proceed with the analytical integration of Eq. 3 over the spatial coordinate r. This leads to the result that links the advective velocity u (the Stefan flow) to the droplet's global mass transfer rate $\dot{m}$:

$$\dot{m} = 4\pi r^2 \rho \mathrm{u}. \tag{5}$$

Then, integrating the simplified species conservation Eq. 4 similarly while substituting the result of Eq. 5 yields the following result for the average molecular velocity of each species, v_i^m:

$$\mathrm{v}_i^m = \frac{\dot{m}_i}{4\pi r^2 \rho Y_i}. \tag{6}$$

Now, from a different perspective, the pair-wise difference of these molecular velocities can also be related to the gradient field of molar fractions ∇X_i through the following relation, obtained from kinetic theory [31]:

$$\nabla X_i = -\sum_{k=1}^{N} \frac{X_i X_k}{\tilde{D}_{i,k}}[\mathbf{v}_i^m - \mathbf{v}_k^m] + (Y_i - X_i)\frac{\nabla \mathbf{p}}{\mathbf{p}} + \frac{\rho}{\mathbf{p}}\sum_{k=1}^{N} Y_i Y_k(\boldsymbol{f}_i - \boldsymbol{f}_k) + \\ + \sum_{k=1}^{N}\left[\left(\frac{X_i X_k}{\rho \tilde{D}_{i,k}}\right)\left(\frac{D_k^T}{Y_k} - \frac{D_i^T}{Y_i}\right)\right]\left(\frac{\nabla T}{T}\right), \tag{7}$$

where $\tilde{D}_{i,k}$ is the binary diffusion coefficient in a multi-component mixture, $\mathbf{p}$ the pressure, $\boldsymbol{f}_i$ the volumetric forces, D_i^T the thermal diffusion coefficient, and T the temperature. The subscript k is used to represent all gaseous species, including i.

To obtain the proposed reference formulation, the following simplifications need to be imposed:

2.4. Low-Mach, dilatable flow i.e. $\nabla \mathbf{p}$=0;

2.5. Negligible volumetric forces i.e. $\boldsymbol{f}_k = 0, \ \forall k$;

2.6. Negligible Soret effects, i.e.:
$\sum_{k=1}^{N}\left[\left(\frac{X_i X_k}{\rho \tilde{D}_{i,k}}\right)\left(\frac{D_k^T}{Y_k} - \frac{D_i^T}{Y_i}\right)\right]\left(\frac{\nabla T}{T}\right) = 0$;

The low-Mach dilatable flow hypothesis removes pressure effects and enforces that the gaseous density only varies with temperature and composition. It is valid for many droplet phase-change applications and is customary in the literature. As for the Soret effect, it has been shown to not be too expressive for most applications concerning droplet phase-change. A useful study can be found, for instance, in [35], where the authors state that even when this effect is not readily negligible, it is often overshadowed by the main term concerning the difference of molecular velocities. This study is also notable in that it browses a wide range of pressures. As for the absence of gravitational effects, this was also discussed in the introduction and is an assumption related to the spherical symmetry. We assume that droplets are small enough such that these effects are small compared to the main term. One way to justify it is through the Bond dimensionless number, which compares surface tension to gravitational forces. Droplets composed of typical fuels will present Bond numbers smaller than 0.01 [52], which indicates that this is typically a relevant assumption. Some studies have been made to better understand the impact of gravitational forces on droplets, for instance, [36].

With these assumptions, Eq. 7 reduces to:

$$\nabla X_i = -\sum_{k=1}^{N} \frac{X_i X_k}{\tilde{D}_{i,k}} [\mathbf{v}_i^m - \mathbf{v}_k^m], \tag{8}$$

and the above result is usually referred to as the Stefan-Maxwell equation. For consistency, if the results of Eqs. 5, 6 are to be used, then the gradient of molar fractions in Eq. 8 above can also be simplified following spherical symmetry:

$$\frac{dX_i}{dr} = -\sum_{k=1}^{N} \frac{X_i X_k}{\tilde{D}_{i,k}} [\mathrm{v}_i^m - \mathrm{v}_k^m]. \tag{9}$$

Substitution of the integration result of species conservation Eq. 6 into the spherical version of the Stefan-Maxwell equations Eq. 9 leads to:

$$4\pi r^2 \rho \frac{dX_i}{dr} = -\sum_{k=1}^{N} \frac{X_i X_k}{\tilde{D}_{i,k}} \left[\frac{\dot{m}_i}{Y_i} - \frac{\dot{m}_k}{Y_k} \right], \tag{10}$$

Now, the presence of a gradient of molar fractions suggests an integration along the radial coordinate r using molar quantities. A molar transfer rate for each species $\dot{n}_i = \dot{m}_i / W_i$ is then introduced,

and converting mass fractions on the RHS to molar fractions leads to:

$$4\pi r^2 c \frac{dX_i}{dr} = -\sum_{k=1}^{N} \frac{[X_k \dot{n}_i - X_i \dot{n}_k]}{\tilde{D}_{i,k}}, \tag{11}$$

where $c = \rho/W$ is the mixture's molar density.

Since when $k = i$ the term in the summation cancels out, Eq. 11 above is also equivalent to:

$$4\pi r^2 c \frac{dX_i}{dr} = -\sum_{\substack{k=1 \\ k\neq i}}^{N} \frac{[X_k \dot{n}_i - X_i \dot{n}_k]}{\tilde{D}_{i,k}}. \tag{12}$$

By making the change of variable $\xi = 1/r$ and by splitting the summation into two different parts, the above equation can be rearranged as:

$$4\pi c \frac{dX_i}{d\xi} = \left[-\sum_{\substack{k=1 \\ k\neq i}}^{N} \frac{\dot{n}_k}{\tilde{D}_{i,k}} \right] X_i + \left[\dot{n}_i \sum_{\substack{k=1 \\ k\neq i}}^{N} \frac{X_k}{\tilde{D}_{i,k}} \right]. \tag{13}$$

Before proceeding to the analytical integration, Eq. 13 can be recast in a matrix form as follows:

$$\frac{d\boldsymbol{X}}{d\xi} = \mathcal{A}\boldsymbol{X}, \tag{14}$$

where $\boldsymbol{X}$ is a column vector for molar fractions of each species i.e. $\boldsymbol{X} = [X_1, X_2, ... X_k, ... X_N]^T$ and the matrix $\mathcal{A}$ is defined as:

$$\mathcal{A} = \frac{1}{4\pi c} \begin{bmatrix} -\sum\limits_{\substack{k=1 \\ k\neq 1}}^{N} \frac{\dot{n}_k}{\tilde{D}_{1,k}} & \frac{\dot{n}_1}{\tilde{D}_{1,2}} & \cdots & \frac{\dot{n}_1}{\tilde{D}_{1,N}} \\ \frac{\dot{n}_2}{\tilde{D}_{2,1}} & -\sum\limits_{\substack{k=1 \\ k\neq 2}}^{N} \frac{\dot{n}_k}{\tilde{D}_{2,k}} & \cdots & \frac{\dot{n}_2}{\tilde{D}_{2,N}} \\ \vdots & \vdots & \ddots & \vdots \\ \frac{\dot{n}_N}{\tilde{D}_{N,1}} & \frac{\dot{n}_N}{\tilde{D}_{N,2}} & \cdots & -\sum\limits_{\substack{k=1 \\ k\neq N}}^{N} \frac{\dot{n}_k}{\tilde{D}_{N,k}} \end{bmatrix} \tag{15}$$

Now, to carry out a simple integration for this system of equations, an additional hypothesis is necessary, customary to droplet mass transfer modeling:

2.7. Constant transport properties (c, $\tilde{D}_{i,k}$) in space;

This hypothesis is customary for droplet heat and mass transfer models, and it is aligned with the same hypothesis used for the energy formulation that will be coupled with this mass transfer result for consistency. In this work, the one-third rule [37], [38] is employed to evaluate said constant properties; however, potential impacts and how to improve on this assumption have also been the focus of the literature as of late; see [39] and [40] for instance. With hypothesis #7, the system of equations Eq. 14 can be integrated straightforwardly to yield:

$$\boldsymbol{\mathcal{X}} = \exp\left[\mathcal{A}\xi\right]\boldsymbol{C} \tag{16}$$

with a suitable constant of integration $\boldsymbol{C}$, which is a second unknown paired with the matrix $\mathcal{A}$.

To proceed with the solution, it is necessary to specify two boundary conditions. First, at the surface of droplet $\xi = 1/R_d$, the molar fractions vector must be $\boldsymbol{\mathcal{X}} = \boldsymbol{\mathcal{X}}^s = [X_1^s, X_2^s, ... X_k^s, ... X_N^s]^T$. The second boundary condition is enforced here using film theory to incorporate convection effects, an important goal for general applications. Namely, at $\xi = 1/(R_d + \delta_{M,max})$, molar fractions must be $\boldsymbol{\mathcal{X}} = \boldsymbol{\mathcal{X}}^\infty = [X_1^\infty, X_2^\infty, ... X_k^\infty, ... X_N^\infty]^T$, with $\delta_{M,max} = \max(\delta_{M,1}, \delta_{M,2}, ... \delta_{M,k}, ... \delta_{M,N})$ with the different δ_M representing the mass transfer boundary layer of each species. In this way, the boundary layer thickness $\delta_{M,max}$ is the largest boundary layer thickness among those of all species, chosen to ensure that all of them have reached the far-away state, i.e., $X_k = X_k^\infty \; \forall k$.

The problem is now reduced to solving the following set of equations simultaneously:

$$\boldsymbol{\mathcal{X}}^s = \exp\left[\frac{1}{R_d}\mathcal{A}\right]\boldsymbol{C}, \tag{17}$$

$$\boldsymbol{\mathcal{X}}^\infty = \exp\left[\frac{1}{(R_d + \delta_{M,max})}\mathcal{A}\right]\boldsymbol{C}. \tag{18}$$

A more practical approach follows if the boundary layer thicknesses are further developed. To do so, the classical boundary layer theory developed in [41] can be used, which has been derived when Stefan flow is not taken into account:

$$\delta_{M,i,0} = \frac{2R_d}{Sh_{i,0} - 2}, \tag{19}$$

where $\delta_{M,i,0}$ is the mass transfer boundary layer thickness when no Stefan flow is present and $Sh_{i,0}$ is the Sherwood number of each species for such a scenario. Since our proposed derivation

includes Stefan flow, the result of Eq. 19 must be corrected for that. The approach we elect to use here is the same as in [42], namely, a correction for the Sherwood number is introduced:

$$Sh^* = 2 + \frac{Sh_0 - 2}{F_M}, \;\; F_M = (1 + B_M)^{0.7} \frac{\ln(1 + B_M)}{B_M}, \tag{20}$$

where B_M is the Spalding mass transfer. The above result was originally employed for a single-component droplet, which means that only a single mass transfer boundary layer was useful, that of the single fuel vapor. In this way, we assume that the proposed correction could also be extended to the boundary layers of each individual species as such:

$$Sh_i^* = 2 + \frac{Sh_{i,0} - 2}{F_{M,i}}, \;\; F_{M,i} = (1 + B_{M,i})^{0.7} \frac{\ln(1 + B_{M,i})}{B_{M,i}}, \tag{21}$$

where the Spalding mass transfer numbers of each species is computed as being:

$$B_{M,i} = \dot{m} \left(\frac{Y_i^s - Y_i^\infty}{\dot{m}_i - \dot{m} Y_i^s} \right). \tag{22}$$

In this way, a corrected version of the boundary layer thickness could be computed through:

$$\delta_{M,i}^* = \frac{2R_d}{Sh_i^* - 2}. \tag{23}$$

The maximum value to be used in Eq. 18 is then computed as $\delta_{max} = 2R_d/(Sh_{min}^* - 2)$, with $Sh_{min}^* = \min(Sh_1^*, Sh_2^*, ... Sh_k^*, ... Sh_N^*)$, leading to:

$$\boldsymbol{\mathcal{X}}^s = \exp\left[\frac{1}{R_d} \mathcal{A} \right] \boldsymbol{C}, \tag{24}$$

$$\boldsymbol{\mathcal{X}}^\infty = \exp\left[\frac{Sh_{min}^* - 2}{Sh_{min}^* R_d} \mathcal{A} \right] \boldsymbol{C}. \tag{25}$$

Once the system is solved and $\mathcal{A}$ is found, molar transfer rates $\dot{n}_k$ are found from its entries, and so the individual mass transfer rates $\dot{m}_k$ follow ($\dot{n}_k = \dot{m}_k / W_k$).

As for the numerical algorithm, the problem is first initialized with the matrix $\mathcal{A}_0^{guess}$ constructed through mass transfer rates computed using any other simpler model. Then, $\boldsymbol{C}_0^{guess}$ can be initialized assuming a non-convective case i.e. $\boldsymbol{C}_0^{guess} = \boldsymbol{\mathcal{X}}_0^\infty$. For subsequent iterations, outputs from the previous iteration are used to construct the arrays $\mathcal{A}^{guess}$, $\boldsymbol{C}^{guess}$. To actually solve the non-linear system, this model was implemented in a Python code and the numerical library "root" from the

SciPy optimize package was utilized. More specifically, the modified Powell method is used to solve the system of equations, called through the MINPACK hybrid routine [43] that numerically computes the Jacobian to minimize the right-hand side of the equation.

Eqs. 24 and 25 represent the final result of the proposed reference strategy. Since the proposed formulation does not make any structural assumptions on diffusion coefficients, it can be compared with other mass transfer models as a reference in this regard. However, as mentioned in the introduction, the analytical integration of the Stefan-Maxwell equations had been previously carried out in [12]. A brief comment is dedicated here to better clarify their differences.

A first limitation of their proposed modeling strategy is the restriction to a single inert species, possibly made to accommodate comparisons with their previous simplified works [11]. Our proposed model, however, follows a derivation procedure that allows multiple inert species to participate, avoiding the necessity of more averaging rules and degrees of freedom, which might obscure the underlying physics. Following this rationale, this more expanded formulation could potentially be used to relax the inert assumption, i.e., no inert species exist. In such a case, molar transfer rates $\dot{n}_i$ are left free to vary for all species, with adequate physical models used to handle the condensation of such species onto the liquid phase. As an additional difference, the result in [12] does not provide any treatment for convection applications which can be limiting. As shown above, our proposed model has also been derived with an analytical integration following the limits of integration of classical boundary layer theory to organically incorporate convection effects, avoiding the introduction of ad-hoc corrections. Finally, in [12], an additional hypothesis was imposed for binary diffusion coefficients that essentially translates to $D_{i,i} = D_{i,\Omega} = D_{\Omega,i}$, where $D_{i,i}$ is the auto-diffusion coefficient for each species i and $D_{i,\Omega}, D_{\Omega,i}$ are the binary diffusion coefficients between each species i and the sole inert species Ω. This hypothesis actually changes the structure of the system of equations, resulting in this final form:

$$4\pi c \frac{d\boldsymbol{\chi}}{d\xi} = \mathcal{A}'\boldsymbol{\chi} + \mathcal{B}', \tag{26}$$

in contrast with our simplified form Eq 26. Not only this hypothesis disrupts the framework of a reference model with respect to the diffusion closure, but, as shown in the results section, can

actually significantly impact calculations.

3. Simplified models and their approach to diffusion

3.1. Extending Law's model: Preferential diffusion

As discussed in the introduction, one of the most used DCMs in the literature today can be traced back to the works of Law [7]. It is the purpose of this section to derive and establish the main characteristics and limitations of this model.

To do that, first, an alternative version of the spherical Stefan-Maxwell is constructed in terms of diffusion velocities for each species, v_i^D. This velocity is defined as the difference between the average molecular velocity and the advective velocity, as follows [31]:

$$\mathbf{v}_i^D = \mathbf{v}_i^m - \mathbf{u}. \tag{27}$$

This means that the difference in molecular velocities between a pair of species is equal to the difference in diffusion velocities of the same pair:

$$\mathbf{v}_i^m - \mathbf{v}_k^m = \mathbf{v}_i^D - \mathbf{v}_k^D. \tag{28}$$

Therefore, the Stefan-Maxwell equations Eq. 8 can also be written in an equivalent form for the difference of diffusion velocities, as such:

$$\nabla X_i = -\sum_{k=1}^{N} \frac{X_i X_k}{\tilde{D}_{i,k}} [\mathbf{v}_i^D - \mathbf{v}_k^D]. \tag{29}$$

Now, to reproduce the structure of Law's results, the supplementary simplification that must be applied is the following:

- Equal diffusion coefficient for all species in the gaseous phase, i.e., $\tilde{D}_{i,k} = \bar{D}$, $\forall i, k$.

Substituting this average diffusion coefficient onto Eq. 29 and rearranging leads to:

$$X_i \mathbf{v}_i^D = X_i \sum_{k=1}^{N} X_k \mathbf{v}_k^D - \bar{D} \nabla X_i. \tag{30}$$

Multiplying the above equation by Y_i/X_i yields:

$$Y_i \mathbf{v}_i^D = Y_i \sum_{k=1}^{N} X_k \mathbf{v}_k^D - \bar{D}\left[Y_i \frac{\nabla X_i}{X_i} \right]. \tag{31}$$

Now, in parallel, it is possible to rewrite a version of Eq. 2 in terms of the diffusion velocity as defined in Eq. 27:

$$\frac{\partial \rho}{\partial t} + \nabla \cdot \left[\rho Y_i \mathbf{u} + \rho Y_i \mathbf{v}_i^D \right] = \dot{\omega}_i. \tag{32}$$

If Eq. 32 above is summed for all species, then global mass conservation must be retrieved, i.e., Eq. 1 must be verified. In this way, the following relation must be true for global mass conservation to be satisfied:

$$\sum_{k=1}^{N} Y_k \mathbf{v}_k^D = 0. \tag{33}$$

Having established the previous result, Eq. 31 is then summed for all species N:

$$\sum_{j=1}^{N} Y_j \mathbf{v}_j^D = \sum_{j=1}^{N} \left[Y_j \sum_{k=1}^{N} X_k \mathbf{v}_k^D \right] - \bar{D} \sum_{j=1}^{N} Y_i \frac{\nabla X_i}{X_i}. \tag{34}$$

At the LHS, we see the result of Eq. 33; Therefore, the LHS must be zero. The first term of the RHS is straightforwardly opened up as follows:

$$\sum_{j=1}^{N} \left[Y_j \sum_{k=1}^{N} X_k \mathbf{v}_k^D \right] = \left[\sum_{j=1}^{N} Y_j \right] \left[\sum_{k=1}^{N} X_k \mathbf{v}_k^D \right] = \sum_{k=1}^{N} X_k \mathbf{v}_k^D. \tag{35}$$

Using both information for the LHS and RHS, Eq. 34 becomes:

$$\sum_{k=1}^{N} X_k \mathbf{v}_k^D = \bar{D}\left[Y_i \frac{\nabla X_i}{X_i} \right]. \tag{36}$$

Eq. 36 above is therefore an expression for the term $\sum_{k=1}^{N} X_k \mathbf{v}_k^D$. The above result can therefore be injected onto the first term of the RHS of Eq. 30 to yield:

$$\mathbf{v}_i^D = \bar{D}\left[\left(\sum_{k=1}^{N} Y_k \frac{\nabla X_k}{X_k} \right) - \frac{\nabla X_i}{X_i} \right] \tag{37}$$

In parallel, the following expression can be developed for the ratio of gradients of molar fractions to molar fractions:

$$\frac{\nabla X_i}{X_i} = \frac{\nabla (Y_i W)}{X_i W_i} = \frac{W \nabla Y_i + Y_i \nabla W}{X_i W_i} = \frac{\nabla Y_i}{Y_i} + \frac{\nabla W}{W}. \tag{38}$$

Substituting this result on Eq. 37 leads to:

$$\mathbf{v}_i^D = \bar{D}\left[\left(\sum_{k=1}^{N}\nabla Y_k\right) + \left(\sum_{k=1}^{N} Y_k \frac{\nabla W}{W}\right) - \frac{\nabla Y_i}{Y_i} - \frac{\nabla W}{W}\right] \tag{39}$$

From Eq. 33, it follows naturally that $\sum_{k=1}^{N}\nabla Y_k = 0$. Furthermore, $\sum_{k=1}^{N} Y_k \frac{\nabla W}{W} = \left(\sum_{k=1}^{N} Y_k\right)\frac{\nabla W}{W} = \frac{\nabla W}{W}$. Then, inside Eq. 39, molar weight terms cancel out, leading to the following formulation:

$$Y_i \mathbf{v}_i^D = -\bar{D}\nabla Y_i. \tag{40}$$

The above equation is almost identical to classical "Fick's Law", which is defined for a binary mixture composed of species $1, 2$ as being, for example:

$$Y_1 \mathbf{v}_1^D = D_{1,2}\nabla Y_1, \tag{41}$$

where $D_{1,2}$ is the binary diffusion coefficient defined between species $1, 2$ in a binary mixture. In this way, the result of Eq. 40 shows that assuming equal diffusion coefficients for all species in the gaseous mixture creates a structural analogy with the pure binary case.

Note that all of these developments do not require the assumption of spherical symmetry. However, to obtain Law's model, an analytical integration is required, and so first spherical symmetry is enforced onto Eq. 40 to obtain:

$$Y_i \mathrm{v}_i^D = -\bar{D}\frac{dY_i}{dr}. \tag{42}$$

Opening up Eq. 4 in terms of diffusion velocities (as done for Eq. 32) and substituting Eq. 42 above as well as Eq. 5 leads to:

$$\frac{d}{dr}\left[\frac{\dot{m}}{4\pi}Y_i - r^2\rho\bar{D}\frac{dY_i}{dr}\right] = 0. \tag{43}$$

This equation represents the difference between gas-phase advective and diffusive fluxes and can be integrated once with respect to the radial coordinate to yield:

$$\dot{m}_i Y_i - 4\pi r^2 \rho \bar{D}\frac{dY_i}{dr} = \dot{m}_i. \tag{44}$$

A second characteristic of Law's strategy relies on defining a representative global fuel vapor mass fraction $\bar{Y}_F$ through:

$$\bar{Y}_F = \sum_{\substack{k=1 \\ k \in \text{vapors}}}^{N} Y_k. \tag{45}$$

Then Eq. 44 can be summed only for the fuel vapor species, leading to:

$$\dot{m}\bar{Y}_F - 4\pi r^2 \rho \bar{D} \frac{dY_F}{dr} = \dot{m}, \tag{46}$$

noting that on the RHS $\sum_{k=1,k\in \text{vapors}}^{N} \dot{m}_k = \sum_{k=1}^{N} \dot{m}_k = \dot{m}$, that is, the global mass transfer rate is retrieved since all remaining species have no contribution to phase-change. As expected, due to the structural similarity of Eq. 40 to the binary case, Eq. 46 is also structurally similar to single-component droplet mass transfer treatments. Rearranging the terms of Eq. 46, a second integration can then be carried out towards a general coordinate R:

$$-4\pi\rho\bar{D} \int_{\bar{Y}_F^s}^{\bar{Y}_F(R)} \frac{d\bar{Y}_F}{1-\bar{Y}_F} = \dot{m} \int_{R_d}^{R} \frac{dr}{r^2}. \tag{47}$$

The integration result can be rearranged as:

$$\dot{m} = 4\pi \left(\frac{1}{\frac{1}{R_d} - \frac{1}{R}} \right) \rho \bar{D} \ln\left(\frac{1-\bar{Y}_F(R)}{1-\bar{Y}_F^s} \right). \tag{48}$$

Notice that at the LHS of Eq. 47, we have an integration of the type $\int dx/x = \ln|x|$ for any x. However, we omit the absolute value operator since it is impossible to have negative values inside the logarithm operator, as it would require mass fractions superior to one, as seen in Eq. 48. Furthermore, the original result was developed for non-convective applications by taking $R \to \infty$, which yields:

$$\dot{m} = 4\pi R_d \rho \bar{D} \ln\left(\frac{1-\bar{Y}_F^\infty}{1-\bar{Y}_F^s} \right). \tag{49}$$

If a Spalding mass transfer representative of all fuel vapors is also defined:

$$\bar{B}_M = \frac{\bar{Y}_F^s - \bar{Y}_F^\infty}{1-\bar{Y}_F^s}, \tag{50}$$

then Eq. 49 assumes its classical form:

$$\dot{m} = 4\pi R_d \rho \bar{D} \ln\left(1 + \bar{B}_M\right). \tag{51}$$

The above results allow for the obtention of the global mass transfer rate of a multi-component droplet. The next step would be to carry out the integration process of each individual species' conservation equations, i.e., Eq. 44 this time around, instead of Eq. 46. This would allow for the

obtention of mass transfer rates of each species, the main characteristic of a DCM. Carrying out the same steps of integration for the species conservation equation of an individual fuel vapor i leads to:

$$\dot{m} = 4\pi R_d \rho \bar{D} \ln\left|1 + B_{M,i}\right|. \tag{52}$$

Note that at the LHS, the global mass transfer rate $\dot{m}$ still appears; the contribution $\dot{m}_i$ from species i is present inside the $B_{M,i}$ term Eq. 22 at the RHS. Also, in contrast with Eq. 51, an absolute value operator is present after integration. This is because, from the definition of $B_{M,i}$ (Eq. 22), it is seen that it is now physically possible to have negative values inside the logarithm term. This happens if either of the following is true for the fractional evaporation rates of each species $\epsilon_i = \dot{m}_i/\dot{m}$:

3.1. $\epsilon_i > Y_i^s$ with $\epsilon_i < Y_i^\infty$;

3.2. $\epsilon_i < Y_i^s$ with $\epsilon_i > Y_i^\infty$.

The integration along the spherical coordinate establishes a monotonically increasing or decreasing profile of mass fractions in case of evaporation or condensation, respectively. Therefore, the two previous conditions can be respectively rephrased as:

3.1. $Y_i^s < \epsilon_i < Y_i^\infty$;

3.2. $Y_i^\infty < \epsilon_i < Y_i^s$.

Since there is no functional a priori connection between fractional evaporation rates and mass fractions, the absolute value operator should be kept for general phase-change cases, where some species might go from evaporation to condensation or vice-versa during the droplet's lifetime.

The final step is to equate Eq. 51 with Eq. 52, and to do that a splitting is needed for each case of the previous conditions. This leads to the following formulation:

$$\dot{m}_i = \dot{m}\left[Y_i^s + \frac{\left(Y_i^s - Y_i^\infty\right)}{\bar{B}_M}\right], \text{if } (1 + B_{M,i}) > 0; \tag{53}$$

$$\dot{m}_i = \dot{m}\left[\frac{Y_i^s\left(1 - \bar{B}_M\right) + Y_i^\infty}{2 + \bar{B}_M}\right], \text{if } (1 + B_{M,i}) < 0. \tag{54}$$

Eq. 53 is the main result of the DCM proposed by Law [1]. Indeed, the original publication did not consider the absolute value operator, which we have deployed here to extend its range of validity through Eq. 54. In the original work [7], the author actually expressed the results in terms of fractional evaporation rates $\epsilon_i = \dot{m}_i/\dot{m}$, and this has been the most used form in the literature. However, we opt to state results here in terms of mass transfer rates directly due to our extension of the model to general condensation scenarios. Indeed, if either an individual species or the global mass transfer behaviors change from evaporation to condensation or vice-versa during the droplet lifetime, an overshoot on the fractional evaporation rate is expected, which is numerically difficult to handle. This was first reported in [13], and the same strategy was employed in [2].

For convective applications, Eq. 47 can be integrated assuming the same treatment as done for Eq. 19, yielding:

$$\dot{m} = 2\pi R_d \rho \bar{D} \bar{Sh}_0 \ln\left(1 + \bar{B}_M\right), \tag{55}$$

where $\bar{Sh}_0$ is the Sherwood number that corresponds to the boundary layer of the representative fuel species assuming that no Stefan flow is present (subscript 0). Then it is possible to also assume that Abramzon and Sirignano's correction would apply here, and the Sherwood number could be corrected as follows:

$$\bar{Sh}^* = 2 + \frac{\bar{Sh}_0 - 2}{\bar{F}_M}, \;\; \bar{F}_M = (1 + \bar{B}_M)^{0.7} \frac{\ln(1 + \bar{B}_M)}{\bar{B}_M}. \tag{56}$$

In this way, the global mass transfer rate Eq. 51 becomes, for general convection applications:

$$\dot{m} = 2\pi R_d \rho \bar{D} \bar{Sh}^* \ln\left(1 + \bar{B}_M\right). \tag{57}$$

Similarly, for such cases the contribution from each species Eq. 52 becomes:

$$\dot{m} = 2\pi R_d \rho \bar{D} Sh_i^* \ln\left|1 + \bar{B}_{M,i}\right|. \tag{58}$$

[1]Note that if $Y_i^\infty = 0$ for all fuels, then $Y_F^\infty = 0$ in Eq. 50; Eq. 53 then degenerates to $\dot{m}_i = \dot{m} Y_i^s / Y_F^s$ or simply $\epsilon_i = Y_i^s / Y_F^s$. This means that each fuel's evaporation participation is simply regulated by their mass participation. This also justifies in [2] why properties that should be computed using fractional evaporation rates can sometimes be computed using mass fractions to a good accuracy.

Now, when equating Eq. 57 with Eq. 58, the equivalent of previous relations Eqs. 53,54 becomes more complex:

$$\dot{m}_i = \dot{m}\left[\frac{Y_i^\infty - Y_i^s\left(1+\bar{B}_M\right)^{\bar{Sh}^*/Sh_i^*}}{1-\left(1+\bar{B}_M\right)^{\bar{Sh}^*/Sh_i^*}}\right], \text{ if } (1+B_{M,i}) > 0; \tag{59}$$

$$\dot{m}_i = \dot{m}\left[\frac{Y_i^\infty + Y_i^s\left(1+\bar{B}_M\right)^{\bar{Sh}^*/Sh_i^*}}{1+\left(1+\bar{B}_M\right)^{\bar{Sh}^*/Sh_i^*}}\right], \text{ if } (1+B_{M,i}) < 0. \tag{60}$$

Following these results, our proposal for the extension of Law's model would, therefore, be able to not only handle general condensation cases (through the absolute value operator splitting) but also would have an organic inclusion of convective effects.

However, when summing for instance the first possibility Eq. 59 for all species, the global mass transfer rate at the LHS cancels out with the multiplicative one at the RHS and the following would have to be true:

$$\sum_{k=1}^{N}\left[\frac{Y_k^\infty - Y_k^s\left(1+\bar{B}_M\right)^{\bar{Sh}^*/Sh_k^*}}{1-\left(1+\bar{B}_M\right)^{\bar{Sh}^*/Sh_k^*}}\right] = 1. \tag{61}$$

There is, however, no structural relationship between $\bar{Sh}^*$ and Sh_i^* that guarantees that Eq. 61 holds, as the average Sherwood number is in itself an additional model to describe the average mass transfer of all individual boundary layers. It is easy to see that the same is true for the second case for the absolute value operator if Eq. 60 is developed instead of Eq. 59. This indicates that the structure of Law's model is not able to organically include convection effects.

To still be able to incorporate convection effects, what is typically done in the literature is to first compute the global mass transfer rate in a convective environment through Eq. 57. Then, individual mass transfer rates $\dot{m}_i$ are computed using the non-convective expressions, Eqs. 53, 54, but with the global mass transfer rate computed with convection. In this way, individual Sherwood numbers for each species Sh_i (and thus, the boundary layer development for each one) play no role, and we can further see another disadvantage when comparing this simplified model with our proposed reference.

3.2. Sacomano et al. model: Differential diffusion

Having introduced the reference model and the proposed extension for Law's model, the comparison with an intermediary model is now more easily justifiable. An intermediary model is here represented through the category of "differential diffusion" models, where the hypothesis of equal diffusion coefficients for each species is relaxed, with Eq. 40 now replaced by:

$$Y_i \mathbf{v}_i^D = -D_i \nabla Y_i, \tag{62}$$

where D_i is a gaseous diffusion coefficient for each species. It is straightforward to see that this strategy is more complex than Law's model since the model would be able to individually characterize the diffusion of each fuel vapor species, even if only toward the whole mixture. To compute such diffusion coefficient, the strategy of Wilke [44], also used in [12] for instance, is here employed:

$$D_i = \frac{(1 - X_i)}{\sum\limits_{\substack{k=1 \\ k \neq i}}^{N} X_k / D_{i,k}}. \tag{63}$$

Then, the mass transfer rates can be computed for convective environments as developed in [13], with the following expressions being the main result:

$$\dot{m}_k = \dot{m} \left(\frac{Y_k^\infty - Y_k^s \exp\left[\frac{\dot{m}}{2\pi R_d Sh_k^* \rho D_k} \right]}{1 - \exp\left[\frac{\dot{m}}{2\pi R_d Sh_k^* \rho D_k} \right]} \right), \text{ if } (1 + B_{M,i}) > 0; \tag{64a}$$

$$\dot{m}_k = \dot{m} \left(\frac{Y_k^\infty + Y_k^s \exp\left[\frac{\dot{m}}{2\pi R_d Sh_k^* \rho D_k} \right]}{1 + \exp\left[\frac{\dot{m}}{2\pi R_d Sh_k^* \rho D_k} \right]} \right), \text{ if } (1 + B_{M,i}) < 0. \tag{64b}$$

It should be highlighted that, as argued in our original work [13], this formulation is also able to organically include convection effects throughout the analytical derivation using boundary layer theory, which is therefore also an advantage when compared to Law's model.

3.3. Complete phase-change strategy: The energy formulation and convection corrections for condensation scenarios

In our previous work [2], we demonstrated that, regardless of the choice for a mass diffusion closure, a general energy model can be derived. Therefore, the final result is also employed here for

all compared mass transfer strategies since it also organically incorporates convection, Stefan flow, general phase-change, and any number of species, which does not create any structural conflict with all presented models. In this way, heat transfer rates $\dot{Q}$ are computed through:

$$\dot{Q} = \frac{\sum_{k=1}^{N} \dot{m}_k c_{p,k}(T^s - T^\infty)}{\exp\left[\frac{\sum_{k=1}^{N} \dot{m}_k c_{p,k}}{2\pi R_d N u^* \lambda}\right] - 1}, \quad \text{if} \quad 1 + B_T > 0, \tag{65a}$$

$$\dot{Q} = -\left(\frac{\sum_{k=1}^{N} \dot{m}_k c_{p,k}(T^s - T^\infty)}{\exp\left[\frac{\sum_{k=1}^{N} \dot{m}_k c_{p,k}}{2\pi R_d N u^* \lambda}\right] + 1}\right), \quad \text{if} \quad 1 + B_T < 0, \tag{65b}$$

where $c_{p,k}$ are specific heats at constant pressure, Nu^* is the corrected Nusselt number computed using a correction for Stefan flow effects analogous to the ones used here for Sherwood numbers, and λ is the thermal conductivity. The Spalding heat transfer number B_T is computed through:

$$B_T = \frac{\sum_{k=1}^{N} \dot{m}_k c_{p,k}(T^s - T^\infty)}{\dot{Q}}. \tag{66}$$

Now, in condensation scenarios, the Spalding transfer number for each species $B_{M,i}$ can become negative and in particular inferior to -1, in which case the Stefan-flow corrections for their corresponding Sherwood numbers would fail; see Eq. 21 for instance. Indeed, originally Abramzon and Sirignano [42] state that their analytical derivation was carried out for $0 < B_M, B_T < 20$, as also observed in [45]. Using a simple analogy from boundary layer theory, it is known that an outward mass flux (evaporation) will tend to stretch the corresponding boundary layer whereas an inward flux (condensation) will tend to compress it [46]. Therefore, we propose the following extension for the correction factors F, to extend the original correction to extreme condensation scenarios:

$$F = (1 + B)^{0.7} \frac{\ln(1 + B)}{B}, \quad \text{if} \quad 0 \leq B < 20, \tag{67}$$

$$F = (1 - B)^{0.7} \frac{\ln(1 - B)}{B} + 2 \quad \text{, if} \quad -20 < B < 0. \tag{68}$$

This extension of the Stefan flow correction can be seen in Fig. 1. Ideally, it would be better to derive from scratch a boundary layer model that is able to transition from condensation to evaporation continuously. However, for a first estimation, we deemed that this correction is satisfactory as it reproduces the global expected physical trends while allowing for the whole mass transfer model to consider Stefan flow effects continuously for consistency.

4. Results

4.1. Model Validation and Benchmarks

The model is first validated against experimental results through the work of Ma et al. [25], and results can be seen in Fig. 2. For this specific validation case, a droplet composed of 6 species was chosen to roughly estimate the characteristics of Diesel fuel. The fuel species are Toluene (C_7H_8), N-decane ($C_{10}H_{22}$), N-dodecane ($C_{12}H_{26}$), N-tetradecane ($C_{14}H_{30}$), N-hexadecane ($C_{16}H_{34}$) and N-octadecane ($C_{18}H_{38}$). In this experiment, droplets of around $80 - 90\mu m$ of initial diameter are suspended in a filament surrounded by hot air at $T^{\infty} = 735K$. It is possible to see an overall good agreement between the proposed model and the experimental data. Differences may be explained by experimental uncertainties, for instance since our model does not include radiation effects nor the heat conduction through the supporting filament. Also, thermodynamic and transport properties are computed using different datasets; our properties are extracted from [47]. Overall, the validation is deemed to be satisfactory.

The proposed model will be compared with Sacomano et al.'s model as well as the proposed extension of Law's model, so it would be useful to have time benchmarks to see how they perform comparatively in terms of computational cost. Using the validation cases of [25], all models were run and benchmarked with a Python in-house code, using a 2.3Ghz 8-core Intel Core i9 processor; the average simulation time was $t_1 = 14.3s$ for the proposed model, $t_2 = 11.6s$ for Sacomano et al.'s model ($t_1/t_2 = 1.23$) and $t = 9.5s$ for Law's model ($t_1/t_3 = 1.51$). This trend is expected, as the proposed model solves a system of equations that is numerically more complex to handle than that of Sacomano et al.'s, whereas Law's model does not require a system of equations altogether.

Next, we show the differences between our proposed model and the one originally published by Tonini and Cossali in [12]. Since the model in [12] is limited to a single inert species and non-convective applications, one such comparison case is selected. In Fig. 3, results are presented for three simulations. At the top, two pure droplets are depicted; to the left is the mass transfer rate for a pure ethanol droplet, and to the right is the mass transfer rate for a pure water droplet. Then, the bottom row is dedicated to a 50%-50% ethanol-water droplet in mass fractions. All simulations have only a single species, air, as the inert one, and with a high-temperature surrounding gas, i.e.,

$T^{\infty} = 1800K$. As expected, both models perform quite similarly for pure conditions (top row). However, for a mixed configuration (bottom row), we see more significant changes in the water mass transfer rate. These may appear to not be as significant, but as seen in the next figures, these can be essentially of the same order as changing completely the mass transfer model to simplified strategies. Recall again that the only difference between both models for non-convective and single-inert cases is the additional hypothesis for binary diffusion coefficients $D_{i,i} = D_{i,\Omega} = D_{\Omega,i}$, with i being any fuel vapor and Ω being the sole inert species. During the demonstration procedure, we showed that this hypothesis is not necessary and, furthermore, that avoiding it leads to a simpler final structure. For the results that follow, scenarios with multiple inert species and/or convection are present, and so we omit further comparisons with the model from [12].

4.2. Comparing different mass transfer models

In sequence, to illustrate the impact of the choice of the mass transfer method, three different liquid mixtures are studied here to represent typical mixtures that may arise for spray combustion applications, for instance. Each simulation tracks the lifetime of a single droplet composed of ethanol and water (E/W), acetone, ethanol, butanol, and water (A/E/B/W), and finally, n-hexane, n-octane, n-decane, and n-dodecane (Alk), with symmetrical initial compositions in mass, as seen in Table 1. For all upcoming figures, the mass transfer strategy presented in this work is labeled as "Reference". Even though the proposed extension of Law's model is used here, our structure is identical to that of Law's when the absolute value is not required. Therefore, in terms of the mass transfer structure, all comparisons here are valid even for users of the original formulation of Law's model - the range of validity is only increased with no compromise. To account for convection in Law's extended model, we use Eq. 57 for the global mass transfer rate and then compute individual mass transfer rates with Eqs. 53 and 54.

For all results that follow, mass fractions at the surface of the droplet were computed with the vapor-liquid equilibrium assumption and employing the activity coefficient method [48], with activity coefficients being computed with the UNIFAC strategy [49]. Also, as customary in the literature, binary diffusion coefficients in the multi-component gaseous mixture are approximated as if a binary mixture, i.e., $\tilde{D}_{i,k} = D_{i,k}$. The proposed models do not need this simplification per

se, but since no practical method for computing $\tilde{D}_{i,k}$ exists to the knowledge of the authors, we compute them as such. A previous study in [50] indicates that this hypothesis is typically valid, but modern treatments on the subject could be envisaged.

In Fig. 4, the baseline case for the E/W droplet is plotted with the far-away state being composed of pure air and the same temperature as the droplet, with no convection. It is possible to see that Sacomano Filho et al.'s model closely follows the reference, whereas Law's model deviates. Particular attention is drawn to the fact that the ethanol mass transfer rate is first underpredicted and then overpredicted, with the inverse behavior observed for water. At the start of the droplet lifetime, these compensate each other, and this information would be lost with a model that does not compute the mass transfer rates of different species. In addition, Law's model tends to predict a longer droplet lifetime, with the ethanol (more volatile species) completely exiting the droplet sooner, when compared to the other models.

In Fig. 5, the same conditions are imposed for the E/W droplet except for the far-away temperature, raised to $T^{\infty} = 1800K$. Once again, Law's model clearly differentiates itself from the other two; this time, however, differences can be seen between the intermediary approach, Sacomano et al.'s model, in comparison to our reference. The same opposed behavior is seen between ethanol and water: underestimated first, then overestimated for ethanol mass transfer rates, and vice-versa for water. The droplet lifetime is nearly identical between all three models; the global mass transfer rate also has an overall similar structure. This raises awareness again of the fact that simple metrics can be deceiving since the availability of different species will be regulated through their individual mass transfer rates.

Moving to Fig. 6, the far-away temperature is changed back to the same as the droplet, but now a convective case is presented, with a far-away velocity of $U^{\infty} = 25m/s$. The initial droplet velocity is still fixed at $U_{d,0} = 0m/s$, but it is left free to vary following a standard drag law for spherical bodies, with a momentum relaxation timescale as in [42]. We see that the physical behavior between individual mass transfer rates is really similar to the one Fig. 4, but more compressed; namely, the under/overshoots are less severe. Still, Law's model predicts a higher droplet lifetime, with the ethanol completely vaporizing earlier than other models.

Finally, in Fig. 7, the baseline case (low temperature, no convection) but with a relative humidity of 80% water at the far-away state instead of pure air is plotted. The humidity is computed using the relative vapor presence ϕ_i^{RVP} parameter as in [2].

In this case, no appreciable differences are visible between the models. A sharp evaporation rate for ethanol at the early stages is coupled with a sharp change from evaporation to condensation for water until the droplet becomes pure water, after which a slow evaporation regime is established.

For the other studied droplets, namely A/E/B/W and Alk, baseline cases are now plotted in Figs. 8 and 9, with the same characteristics as the baseline E/W droplet but with compositions as listed in Table 1. At the lower left quadrant of Fig 8, evaporation for the most volatile species (acetone and ethanol) seems to be accurately reproduced among all three models. However, at the lower right quadrant, we see that Law's model predicts an undershoot followed by an overshoot for the computation of butanol's mass transfer rates and the opposite behavior for water. These differences cancel out and predict similar global mass transfer rates and droplet lifetimes. As for the Alk configuration, no substantial difference is seen between the models in any particular metric.

Now, in Figs. 10 and 11 the surrounding temperature is once again raised to $T^{\infty} = 1800K$. Once again, we see that the temperature tends to increase discrepancies between models, specifically for mass transfer rates of individual species. Differences between Sacomano et al.'s formulation and the reference tend to be limited, whereas Law's model again tends to present higher deviations for the least volatile species, butanol and water. Once again, no appreciable difference is seen for the alkane mixture, as seen in Fig. 11.

As for the convective and humidity cases, we opt to omit them for conciseness since the conclusions follow the same trends as those presented for the E/W droplet. In general, Law's model tends to approximate the most toward the reference formulation for alkane mixtures. Therefore, for users that expect to work only with such mixtures, it could still be a viable option, provided that the droplets are not expected to drastically change their composition during their lifetime (if, for instance, gaseous species that were not originally present in the droplets are allowed to condensate toward them). However, for multi-component mixtures containing ketones and/or alcohols, the

use of more robust models is advised since differences can become significant, especially for the prediction of individual mass transfer rates. This could severely impact the prediction of a flame structure through fuel availability.

To approach conditions more representative of what a droplet might face in spray combustion scenarios, we conduct an extra simulation using the framework first developed in [2]. Namely, a one-dimensional premixed laminar flame is generated following an analytical treatment. In this setup, as the droplet moves, it encounters varying conditions at the faraway state for temperature, composition, and velocity instead of fixed ones. Results are shown for the E/W droplet in Fig. 12, including the profiles generated by the flame in temperature and mass fractions. It is directly possible to see that little difference is present in global mass transfer rates and the variation of the droplet's diameter squared. As for the species, the main difference is observed for the water mass transfer rates; all models predict roughly the same physics, but Law's model presents higher, then lower evaporation rates than the reference. The model of Sacomano Filho et al., in contrast, exhibits an intermediary behavior closer to that of the reference.

Now in Fig. 13 it is possible to see the A/E/B/W droplet now exposed to the same Ethanol stoichiometric flame. No major differences can be observed concerning global quantities, except for the end of the droplet lifetime; it is possible to see that Law's model simply misses some part of the physics therein. Upon further inspection, it is possible to see a sharp contrast between the behavior of Law's model and the two others especially concerning the Butanol and Water species. The complex physical behavior missed by Law's model is the sharp valley on Butanol's evaporation rate showcased by the two other models, which actually indicates a premature complete evaporation of Water and thus a droplet composed only of butanol towards the end of its lifetime, whereas Law's model predicts the opposite, with a quite complex zig-zag motion on water's evaporation rate toward the end. A small difference can also be observed considering the minimum value of Ethanol's evaporation rate, which is roughly the same between both simplified models and different compared to the reference. A flame configuration was also run for the Alk droplet, this time using a n-hexane flame, but no appreciable difference can be seen between all three models. This would indicate that discrepancies tend to be higher for mixtures containing substances

that interact with water and that also present more complex vapor-liquid equilibriums (typically, activity coefficients farther away from unity).

As seen in the previous figures, for most scenarios, Sacomano et al's model tends to closely follow the proposed reference model. Differences tend to appear in a more pronounced fashion as the surrounding conditions get more complex; this will be the case for, e.g., reactive flows and spray combustion Since the computational overhead is not too great, it is recommended that this model be at least tested for a particular droplet phase-change application to see if the additional physics are relevant. This is especially recommended to users who still are using some version of Law's model; as discussed in the literature, many different versions of the same result are widely in use, and progressing to this more complex model might be valuable.

5. Summary and conclusions

In this work, a mass transfer formulation for droplet general phase-change with no structural constraints concerning diffusion coefficients was derived and investigated in diverse conditions. This formulation was based on the analytical integration of the Stefan-Maxwell equations following fundamental simplifications which are common to all mass transfer models in the literature. The hypothesis and simplications adopted during the derivation process, as well as the obtained results, allow us to conclude that the proposed formulation can be used as a reference concerning the diffusion modeling, the main driver for droplet phase-change.

To corroborate this, it was demonstrated that one of the most used droplet evaporation results, the one developed originally by Law [7], requires the assumption of equal diffusion coefficients for all gaseous species, whereas other intermediary treatments, such as those in [9, 10, 11, 13] all require the computation of a new diffusion coefficient between each species and their surrounding mixture. This is in contrast with the proposed reference model, which requires no simplifications for the mass diffusion closure, its main feature. As a second feature, the final formulation is also developed to avoid restrictions on the number of fuel and inert species. Another benefit that contributes to the rigor of the proposed model is the fact that boundary layer effects are included organically, and an extension based on a physical interpretation of the boundary layer is included to allow the

film thickness correction for general evaporation and condensation mechanisms. In particular, it was also demonstrated that Law's formulation, although frequently used, cannot organically incorporate convection effects; this must be done in analogy with the single-component case, which is not the case for the reference formulation.

To allow for the comparison between modeling strategies throughout the paper, the general energy formulation demonstrated in [2] was employed. The proposed model was first validated through a comparison with experimental data for droplets composed of Diesel fuels from [25]. Benchmarks showed that for this validation case, a factor of around $1.5x$ is the maximum extra computational cost of using the proposed formulation when compared to both other mass transfer strategies. The model is also briefly compared to the one of [51]. Then, simulations were run for three types of droplets: ethanol / water, acetone / ethanol / butanol / water, and n-hexane / n-octane / n-decane / n-dodecane to represent typical mixtures in spray combustion applications. The effects of temperature, surrounding composition, and velocity were first isolated and then mixed together following a surrounding laminar flame profile obtained from stoichiometric analytical results as done previously in [2]. In general, it was seen that Law's model systematically deviated more in comparison with the two other models, often predicting completely different physics. This was mainly limited to mixtures that contained fuels that interacted with water and presented larger deviations from the ideal vapor-liquid equilibrium (Raoult's law). Representing an intermediate class of mass transfer formulations, the model proposed in [13] delivered results with a generally satisfactory agreement with the reference formulation. Deviations become more noticeable when varying surrounding conditions are imposed on the droplet, highlighting a potential sensibility for more complex applications. For mixtures containing only alkanes, all models behaved in a similar fashion. Therefore, one of the main takeaways is that, even though Law's formulation has the advantage of its simplified formulation, care must be taken when employing it for general mixtures, at least in comparison with such models.

From perspectives in this field, the first important task concerns relaxing even more the restrictions on the diffusion mechanism through the binary diffusion coefficients $\tilde{D}_{i,k}$. Indeed, these have been historically computed as being those between a pair of species in a binary mixture and not the

real multi-component diffusion coefficients, where the interaction between the pairs is affected by the presence of other molecules. For such an endeavor, a strategy could be to use semi-empirical models, such as the Chapman-Enskog formalism, as seen, for instance, in [48]. Also, another possibility is to conduct a study using this reference model to evaluate if the average diffusion coefficients $\bar{D}$ and D_i used for Sacomano et al.'s and Law's model, respectively, can be calibrated to yield accurate results with less computational cost. Also, since all of the proposed formulations were obtained through analytical integrations for the gaseous phase, there is no impediment to coupling this model with a finer description of the droplet's interior. A useful starting framework can be found in [8], where a theoretical solution is proposed for the temperature diffusion equation, analogous to the species's equations for this simplified case. We reiterate that all of the above propositions could be coupled with no restrictions with the general energy formulation of [2]. Notably, Soret effects thermodiffusion effects could also be studied in this framework, further incorporating features that impact mass diffusion. Following the treatment done in [14] to extend the previous model [12] toward spheroidal shapes, theoretically, the same could be done with this reference model, with perhaps a greater challenge considering the organic incorporation of boundary layer effects and the Stefan flow effect onto said boundary layers, for general convective applications. It would also be ideal to develop an analytical or numerical correlation to rigorously incorporate Stefan flow effects for general phase-change scenarios. Finally, an important perspective is the comparison of different mass transfer strategies on two-way frameworks, ideally for complex flows, e.g., with combustion. This would further indicate whether other strategies perform similarly to the proposed reference and would provide computation benchmarks that are more useful to the interested user.

6. Acknowledgements

Support from the French Agence Nationale de la Recherche (ANR) in the MIMETYC project (grant ANR-17-CE22-0003) is acknowledged. We also acknowledge the financial support from the São Paulo Research Foundation (FAPESP - grant 2021/14245-1) and the Coordenação de Aperfeiçoamento de Pessoal de Nível Superior – Brasil (CAPES) – Finance Code 001.

References

[1] G. M. Faeth, Current status of droplet and liquid combustion, Prog. Energy Combust. Sci. 3 (4) (1977) 191–224. doi:10.1016/0360-1285(77)90012-0.
URL http://linkinghub.elsevier.com/retrieve/pii/0360128577900120

[2] A. Carvalho Santos, F. L. Sacomano Filho, A. Vié, The general formulation of the energy equation and the impact of enthalpy diffusion on multi-component droplet heat and mass transfer, International Journal of Heat and Mass Transfer 210 (2023) 124172. doi:10.1016/j.ijheatmasstransfer.2023.124172.
URL https://linkinghub.elsevier.com/retrieve/pii/S0017931023003253

[3] B. J. Wood, H. Wise, S. H. Inami, Heterogeneous combustion of multicomponent fuels, Combustion and Flame 4 (C) (1960) 235–242. doi:10.1016/s0010-2180(60)80027-2.

[4] C. K. Law, H. K. Law, d2-LAW FOR MULTICOMPONENT DROPLET VAPORIZATION AND COMBUSTION., AIAA Paper 20 (4) (1981) 522–527. doi:10.2514/6.1981-264.

[5] O. S. Abianeh, C. P. Chen, A discrete multicomponent fuel evaporation model with liquid turbulence effects, International Journal of Heat and Mass Transfer 55 (23-24) (2012) 6897–6907. doi:10.1016/j.ijheatmasstransfer.2012.07.003.
URL http://dx.doi.org/10.1016/j.ijheatmasstransfer.2012.07.003

[6] W. A. Sirignano, Fluid Dynamics and Transport of Droplets and Sprays, second edi Edition, Cambridge University Press, New York, NY, 2010. arXiv:arXiv:1011.1669v3, doi:10.1115/1.483244.

[7] C. K. Law, Multicomponent droplet combustion with rapid internal mixing, Combustion and Flame 26 (C) (1976) 219–233. doi:10.1016/0010-2180(76)90073-0.

[8] S. S. Sazhin, Droplets and Sprays: Simple Models of Complex Processes, Springer, 2022. doi:https://doi.org/10.1007/978-3-030-99746-5.

[9] V. Ebrahimian, C. Habchi, Towards a predictive evaporation model for multi-component hydrocarbon droplets at all pressure conditions, International Journal of Heat and Mass Transfer 54 (15-16) (2011) 3552–3565. doi:10.1016/j.ijheatmasstransfer.2011.03.031.
URL http://dx.doi.org/10.1016/j.ijheatmasstransfer.2011.03.031

[10] L. Zhang, S.-C. Kong, Multicomponent vaporization modeling of bio-oil and its mixtures with other fuels, Fuel 95 (2012) 471–480. doi:10.1016/j.fuel.2011.12.009.

[11] S. Tonini, G. E. Cossali, A novel formulation of multi-component drop evaporation models for spray applications, International Journal of Thermal Sciences 89 (2015) 245–253. doi:10.1016/j.ijthermalsci.2014.10.016.
URL http://dx.doi.org/10.1016/j.ijthermalsci.2014.10.016

[12] S. Tonini, G. E. Cossali, A multi-component drop evaporation model based on analytical solution of Stefan-Maxwell equations, International Journal of Heat and Mass Transfer 92 (2016) 184–189. doi:10.1016/j.

ijheatmasstransfer.2015.08.014.
URL http://dx.doi.org/10.1016/j.ijheatmasstransfer.2015.08.014

[13] F. L. Sacomano Filho, A. Carvalho Santos, A. Vié, G. C. Krieger Filho, A new robust modeling strategy for multi-component droplet heat and mass transfer in general ambient conditions, International Journal of Heat and Mass Transfer 194 (2022) 123102. doi:10.1016/j.ijheatmasstransfer.2022.123102.
URL https://doi.org/10.1016/j.ijheatmasstransfer.2022.123102

[14] S. Tonini, G. E. Cossali, An analytical model for the evaporation of multi-component spheroidal drops based on Stefan–Maxwell equations, International Journal of Thermal Sciences 171 (August 2021) (2022) 107223. doi:10.1016/j.ijthermalsci.2021.107223.
URL https://doi.org/10.1016/j.ijthermalsci.2021.107223

[15] T. W. Park, S. K. Aggarwal, V. R. Katta, Gravity effects on the dynamics of evaporating droplets in a heated jet, Journal of Propulsion and Power 11 (3) (1995) 519–528. doi:10.2514/3.23873.

[16] S. Tonini, G. E. Cossali, Modeling the evaporation of sessile drops deformed by gravity on hydrophilic and hydrophobic substrates, Physics of Fluids 35 (3) (mar 2023). doi:10.1063/5.0143575.

[17] F. L. Sacomano Filho, G. C. Krieger Filho, J. A. van Oijen, A. Sadiki, J. Janicka, A novel strategy to accurately represent the carrier gas properties of droplets evaporating in a combustion environment, International Journal of Heat and Mass Transfer 137 (2019) 1141–1153. doi:10.1016/j.ijheatmasstransfer.2019.03.164.
URL https://doi.org/10.1016/j.ijheatmasstransfer.2019.03.164

[18] G. Lupo, C. Duwig, Uncertainty quantification of multispecies droplet evaporation models, International Journal of Heat and Mass Transfer 154 (2020). doi:10.1016/j.ijheatmasstransfer.2020.119697.

[19] S. K. Aggarwal, H. C. Mongia, Multicomponent and high-pressure effects on droplet vaporization, Journal of Engineering for Gas Turbines and Power 124 (2) (2002) 248–255. doi:10.1115/1.1423640.

[20] S. S. Sazhin, A. Elwardany, P. A. Krutitskii, G. Castanet, F. Lemoine, E. M. Sazhina, M. R. Heikal, A simplified model for bi-component droplet heating and evaporation, International Journal of Heat and Mass Transfer 53 (21-22) (2010) 4495–4505. doi:10.1016/j.ijheatmasstransfer.2010.06.044.
URL http://dx.doi.org/10.1016/j.ijheatmasstransfer.2010.06.044

[21] A. Bader, P. Keller, C. Hasse, The influence of non-ideal vapor-liquid equilibrium on the evaporation of ethanol/iso-octane droplets, International Journal of Heat and Mass Transfer 64 (2013) 547–558. doi:10.1016/j.ijheatmasstransfer.2013.04.056.
URL http://dx.doi.org/10.1016/j.ijheatmasstransfer.2013.04.056

[22] C. Wang, A. M. Dean, H. Zhu, R. J. Kee, The effects of multicomponent fuel droplet evaporation on the kinetics of strained opposed-flow diffusion flames, Combustion and Flame 160 (2) (2013) 265–275. doi:10.1016/j.combustflame.2012.10.012.

[23] P. Keller, T. Knorsch, M. Wensing, C. Hasse, Experimental and numerical analysis of iso-octane/ethanol sprays

under gasoline engine conditions, International Journal of Heat and Mass Transfer 84 (2015) 497–510. doi:10.1016/j.ijheatmasstransfer.2015.01.011.
URL http://dx.doi.org/10.1016/j.ijheatmasstransfer.2015.01.011

[24] K. Han, G. Song, X. Ma, B. Yang, An experimental and theoretical study of the effect of suspended thermocouple on the single droplet evaporation, Applied Thermal Engineering 101 (2016) 568–575. doi:10.1016/j.applthermaleng.2015.12.022.
URL http://dx.doi.org/10.1016/j.applthermaleng.2015.12.022

[25] X. Ma, F. Zhang, K. Han, G. Song, Numerical modeling of acetone-butanol-ethanol and diesel blends droplet evaporation process, Fuel 174 (2016) 206–215. doi:10.1016/j.fuel.2016.01.091.

[26] S. S. Sazhin, Modelling of fuel droplet heating and evaporation: Recent results and unsolved problems, Fuel 196 (2017) 69–101. doi:10.1016/j.fuel.2017.01.048.
URL http://dx.doi.org/10.1016/j.fuel.2017.01.048

[27] T. T. Nguyen, S. Mitra, M. J. Sathe, V. Pareek, J. B. Joshi, G. M. Evans, Evaporation of a suspended binary mixture droplet in a heated flowing gas stream, Experimental Thermal and Fluid Science 91 (June 2017) (2018) 329–344. doi:10.1016/j.expthermflusci.2017.10.025.
URL https://doi.org/10.1016/j.expthermflusci.2017.10.025

[28] S. Shen, Z. Che, T. Wang, Z. Yue, K. Sun, S. Som, A model for droplet heating and evaporation of water-in-oil emulsified fuel, Fuel 266 (October 2019) (2020) 116710. doi:10.1016/j.fuel.2019.116710.
URL https://doi.org/10.1016/j.fuel.2019.116710

[29] V. Shastry, Q. Cazeres, B. Rochette, E. Riber, B. Cuenot, Numerical study of multicomponent spray flame propagation, Proceedings of the Combustion Institute 38 (2) (2021) 3201–3211. doi:10.1016/j.proci.2020.07.090.
URL https://doi.org/10.1016/j.proci.2020.07.090

[30] W. Yang, J. Xia, X. Y. Wang, K. D. Wan, A. Megaritis, H. Zhao, Predicting evaporation dynamics of a multicomponent gasoline/ethanol droplet and spray using non-ideal vapour-liquid equilibrium models, International Journal of Heat and Mass Transfer 168 (2021) 120876. doi:10.1016/j.ijheatmasstransfer.2020.120876.
URL https://doi.org/10.1016/j.ijheatmasstransfer.2020.120876

[31] R. B. Bird, W. E. Stewart, E. N. Lightfoot, D. J. Klingenberg, Introductory Transport Phenomena, Wiley, 2015.

[32] F. Mashayek, Dynamics of evaporating drops. Part I: Formulation and evaporation model, International Journal of Heat and Mass Transfer 44 (8) (2001) 1517–1526. doi:10.1016/S0017-9310(00)00199-X.

[33] S. S. Sazhin, P. A. Krutitskii, I. G. Gusev, M. R. Heikal, Transient heating of an evaporating droplet, International Journal of Heat and Mass Transfer 53 (13-14) (2010) 2826–2836. doi:10.1016/j.ijheatmasstransfer.2010.02.015.
URL http://dx.doi.org/10.1016/j.ijheatmasstransfer.2010.02.015

[34] P. Jenny, D. J. E. M. Roekaerts, N. Beishuizen, Modeling of turbulent dilute spray combustion, Prog. Energy Combust. Sci. 38 (6) (2012) 846–887. doi:10.1016/j.pecs.2012.07.001.
URL http://linkinghub.elsevier.com/retrieve/pii/S0360128512000445

[35] K. Harstad, J. Bellan, Evaluation of commonly used assumptions for isolated and cluster heptane drops in nitrogen at all pressures, Combustion and Flame 127 (1-2) (2001) 1861–1879. doi:10.1016/S0010-2180(01)00292-9.

[36] C. Habchi, V. Ebrahimian, Gravitational effects on multi-component droplet evaporation, Microgravity Science and Technology 24 (3) (2012) 229–235. doi:10.1007/s12217-012-9303-z.

[37] G. L. Hubbard, V. E. Denny, A. F. Mills, Droplet evaporation: Effects of transients and variable properties, Int. J. Heat Mass Transf. 18 (9) (1975) 1003–1008. doi:10.1016/0017-9310(75)90217-3.

[38] M. C. Yuen, L. W. Chen, On Drag of Evaporating Liquid Droplets, Combustion Science and Technology 14 (4-6) (1976) 147–154. doi:10.1080/00102207608547524.

[39] G. E. Cossali, S. Tonini, An analytical model of heat and mass transfer from liquid drops with temperature dependence of gas thermo-physical properties, International Journal of Heat and Mass Transfer 138 (2019) 1166–1177. doi:10.1016/j.ijheatmasstransfer.2019.04.066.

[40] J. Finneran, On the evaluation of transport properties for droplet evaporation problems, International Journal of Heat and Mass Transfer 181 (2021) 121858. doi:10.1016/j.ijheatmasstransfer.2021.121858.
URL https://doi.org/10.1016/j.ijheatmasstransfer.2021.121858

[41] D. B. Spalding, The Combustion of Liquid Fuels, Symposium (international) on combustion 4 (1953) 847–864.

[42] B. Abramzon, W. A. Sirignano, Droplet vaporization model for spray combustion calculations, Int. J. Heat Mass Transf. 32 (9) (1989) 1605–1618. doi:10.1016/0017-9310(89)90043-4.
URL http://linkinghub.elsevier.com/retrieve/pii/0017931089900434

[43] J. Moré, B. Garbow, K. Hillstrom, User guide for MINPACK-1 (1980).

[44] D. F. Fairbanks, C. R. Wilke, Diffusion Coefficients in Multicomponent Gas Mixtures, Industrial & Engineering Chemistry 42 (3) (1950) 471–475. doi:10.1021/ie50483a022.

[45] S. S. Sazhin, Advanced models of fuel droplet heating and evaporation, Progress in Energy and Combustion Science 32 (2) (2006) 162–214. doi:10.1016/j.pecs.2005.11.001.

[46] H. Schlichting, K. Gersten, Boundary-Layer Theory, 9th Edition, Springer, 2017.

[47] VDI e. V. (Ed.), VDI Heat Atlas, 2nd Edition, Springer, 2010. doi:10.1007/978-3-540-77877-6.

[48] B. Poling, J. M. Prausnitz, J. P. O'Connell, The properties of gases and liquids, 5th Edition, McGRAW-HILL, 2001.

[49] A. Fredenslund, R. L. Jones, J. M. Prausnitz, Group-contribution estimation of activity coefficients in nonideal liquid mixtures, AIChE Journal 21 (6) (1975) 1086–1099. doi:10.1002/aic.690210607.

[50] S. I. Sandler, E. A. Mason, Kinetic-theory deviations from blanc's law of ion mobilities, The Journal of Chemical

Physics 48 (7) (1968) 2873–2875. doi:10.1063/1.1669546.

[51] P. Talbot, B. Sobac, A. Rednikov, P. Colinet, B. Haut, Thermal transients during the evaporation of a spherical liquid drop, International Journal of Heat and Mass Transfer 97 (2016) 803–817. doi:10.1016/j.ijheatmasstransfer.2015.12.075.
URL http://dx.doi.org/10.1016/j.ijheatmasstransfer.2015.12.075

[52] Artur Carvalho Santos, On the modelling of heat and mass transfer for multi-component droplets, Ph.D. thesis (2022).
URL https://www.theses.fr/2022UPAST157

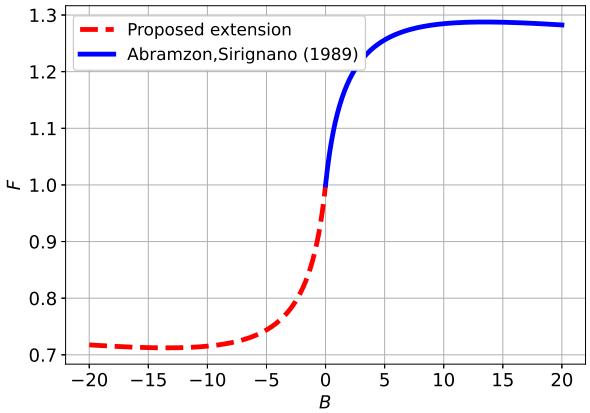

Figure 1: Correction factors for boundary layer under evaporation/condensation regimes following Eqs. 67 (blue) and 68 (red).

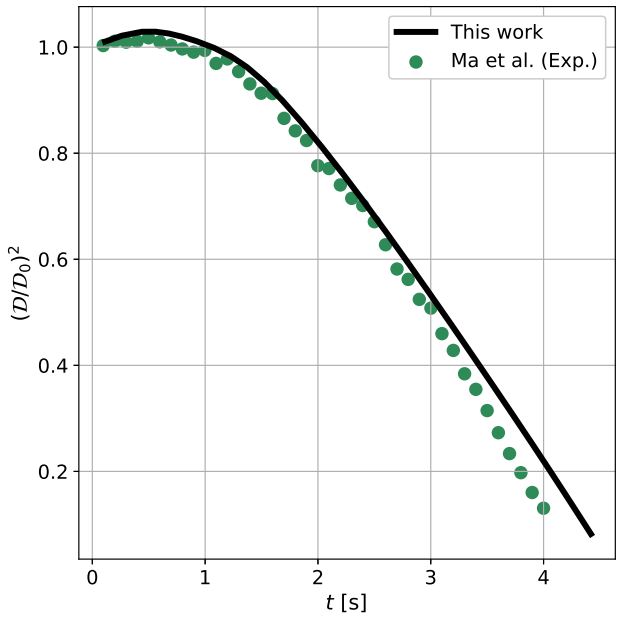

Figure 2: Normalized diameter squared $(\mathcal{D}/\mathcal{D}_0)^2$ versus time $t/\mathcal{D}_0^2$ for a Diesel droplet composed of the following initial mass fractions $Y_{C_7H_8} = 0.08$, $Y_{C_{10}H_{22}} = 0.11$, $Y_{C_{12}H_{26}} = 0.21$, $Y_{C_{14}H_{30}} = 0.27$, $Y_{C_{16}H_{34}} = 0.17$ and $Y_{C_{18}H_{38}} = 0.16$. Experimental data extracted from [25]. For this simulation, $\mathcal{D}_0 = 80\mu m$, $T_{d,0} = 300K$, $T^\infty = 723K$, $U_{d,0} = 0m/s$, $U^\infty = 0m/s$ and the far-away state is composed of pure air.

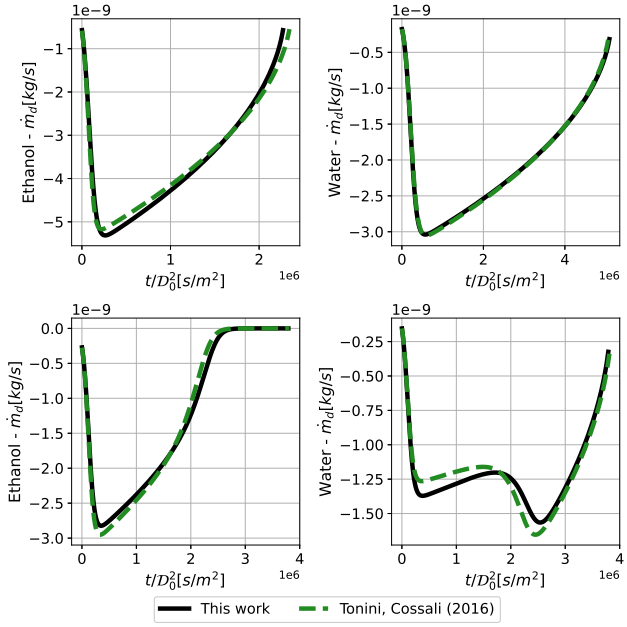

Figure 3: Top-left: Water mass transfer rate $\dot{m}_k$ versus reduced time $t/\mathcal{D}_0^2$ for a pure water droplet. Top-right: Ethanol mass transfer rate $\dot{m}_k$ versus reduced time $t/\mathcal{D}_0^2$ for a pure ethanol droplet. Bottom row: Ethanol and water mass transfer rates $\dot{m}_k$ versus reduced time $t/\mathcal{D}_0^2$ for a 50%/50% ethanol-water droplet. For all cases, $\mathcal{D}_0 = 20\mu m$, $T_{d,0} = 300K$, $T^\infty = 1800K$, $U_{d,0} = 0m/s$, $U^\infty = 0m/s$ and the far-away state is composed of pure air.

Droplet	Initial composition (mass fractions)
E/W	$[C_2H_5OH] = 0.5$, $[H_2O] = 0.5$
A/E/B/W	$[C_3COCH_3] = 0.25$, $[C_2H_5OH] = 0.25$, $[C_4H_9OH] = 0.25$, $[H_2O] = 0.25$
Alk	$[C_6H_{16}] = 0.25$, $[C_8H_{18}] = 0.25$, $[C_{10}H_{22}] = 0.25$, $[C_{12}H_{26}] = 0.25$

Table 1: Initial droplet compositions in mass fractions used in the numerical investigations of this section. "E/W" refers to ethanol/water, "A/E/B/W" to acetone/ethanol/butanol/water, and "Alk" to n-hexane/n-octane/n-decane/n-dodecane.

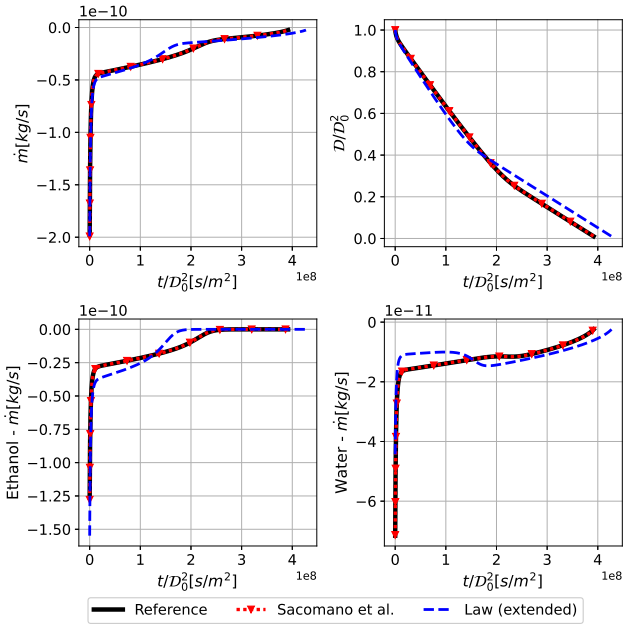

Figure 4: Ethanol/water (E/W) droplet with $\mathcal{D}_0 = 20\mu m$, $T_{d,0} = 300K$, $T^\infty = 300.01K$, $U_{d,0} = 0m/s$, and $U^\infty = 0m/s$. The far-away state is composed of pure air. Results are displayed for the global mass transfer rate $\dot{m}$, the normalized diameter squared $(\mathcal{D}/\mathcal{D}_0)^2$ and individual mass transfer rates $\dot{m}_k$ for each species, versus a reduced time $t/\mathcal{D}_0^2$.

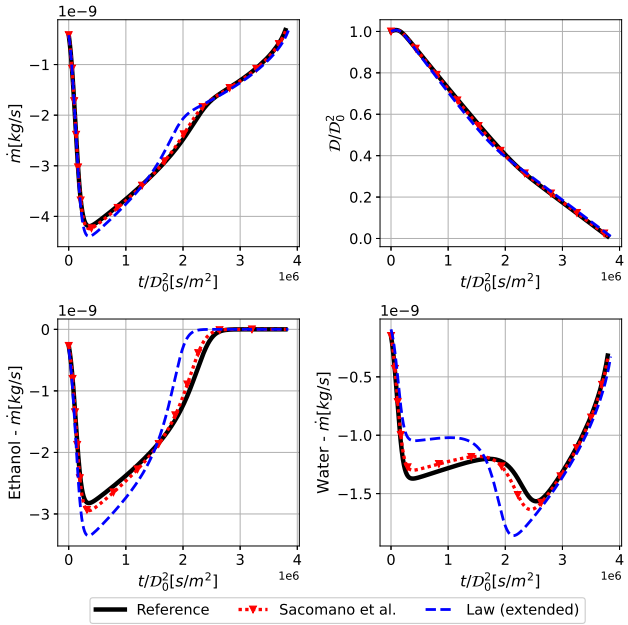

Figure 5: Ethanol/water (E/W) droplet with $\mathcal{D}_0 = 20\mu m$, $T_{d,0} = 300K$, $T^\infty = 1800K$, $U_{d,0} = 0m/s$, and $U^\infty = 0m/s$. The far-away state is composed of pure air. Results are displayed for the global mass transfer rate $\dot{m}$, the normalized diameter squared $(\mathcal{D}/\mathcal{D}_0)^2$ and individual mass transfer rates $\dot{m}_k$ for each species, versus a reduced time $t/\mathcal{D}_0^2$.

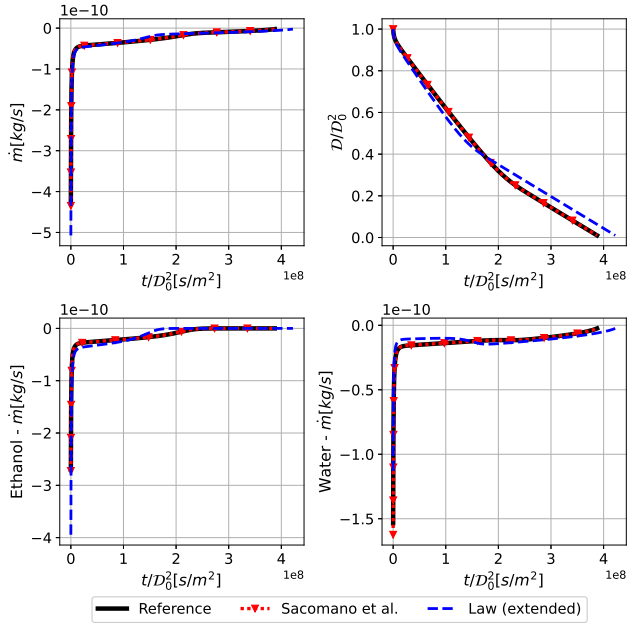

Figure 6: Ethanol/water (E/W) droplet with $\mathcal{D}_0 = 20\mu m$, $T_{d,0} = 300K$, $T^\infty = 300.01K$, $U_{d,0} = 0m/s$, and $U^\infty = 25m/s$. The far-away state is composed of pure air. Results are displayed for the global mass transfer rate $\dot{m}$, the normalized diameter squared $(\mathcal{D}/\mathcal{D}_0)^2$ and individual mass transfer rates $\dot{m}_k$ for each species, versus a reduced time $t/\mathcal{D}_0^2$.

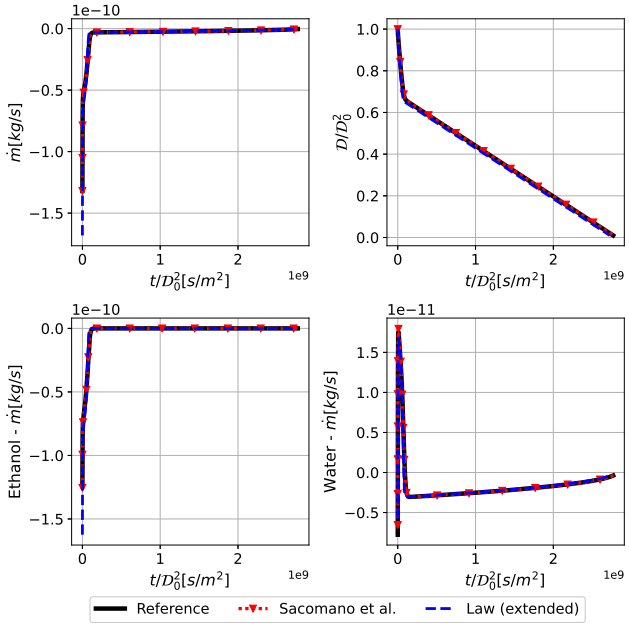

Figure 7: Ethanol/water (E/W) droplet with $\mathcal{D}_0 = 20\mu m$, $T_{d,0} = 300K$, $T^\infty = 300.01K$, $U_{d,0} = 0m/s$, and $U^\infty = 0m/s$. The far-away state is composed of a mixture of air and water at 80% humidity. Results are displayed for the global mass transfer rate $\dot{m}$, the normalized diameter squared $(\mathcal{D}/\mathcal{D}_0)^2$ and individual mass transfer rates $\dot{m}_k$ for each species, versus a reduced time $t/\mathcal{D}_0^2$.

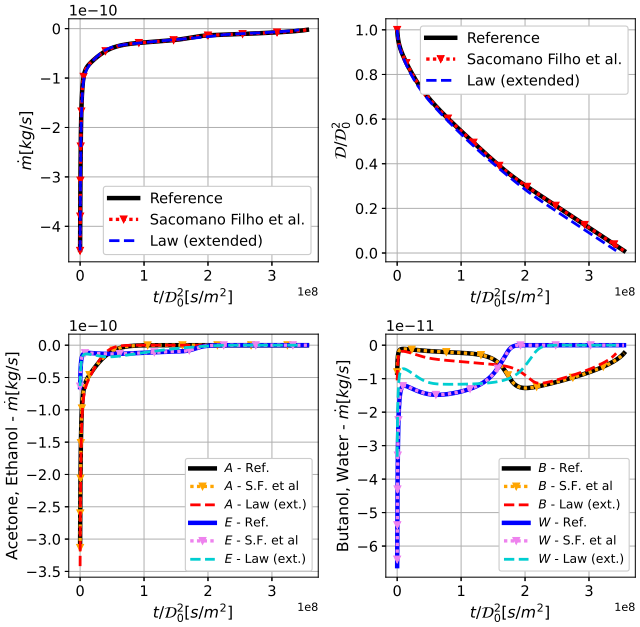

Figure 8: Acetone/ethanol/butanol/water (A/E/B/W) droplet with $\mathcal{D}_0 = 20\mu m$, $T_{d,0} = 300K$, $T^\infty = 300.01K$, $U_{d,0} = 0m/s$, and $U^\infty = 0m/s$. The faraway state is composed of pure air. Results are displayed for the global mass transfer rate $\dot{m}$, the normalized diameter squared $(\mathcal{D}/\mathcal{D}_0)^2$ and individual mass transfer rates $\dot{m}_k$ for each species, versus a reduced time $t/\mathcal{D}_0^2$.

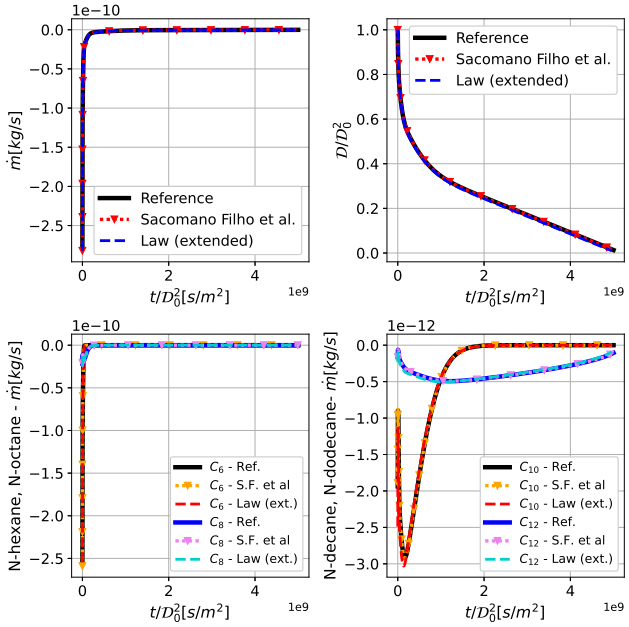

Figure 9: N-hexane/N-octane/N-decane/N-dodecane (Alk) droplet with $\mathcal{D}_0 = 20\mu m$, $T_{d,0} = 300K$, $T^\infty = 300.01K$, $U_{d,0} = 0m/s$, and $U^\infty = 0m/s$. The faraway state is composed of pure air. Results are displayed for the global mass transfer rate $\dot{m}$, the normalized diameter squared $(\mathcal{D}/\mathcal{D}_0)^2$ and individual mass transfer rates $\dot{m}_k$ for each species, versus a reduced time $t/\mathcal{D}_0^2$.

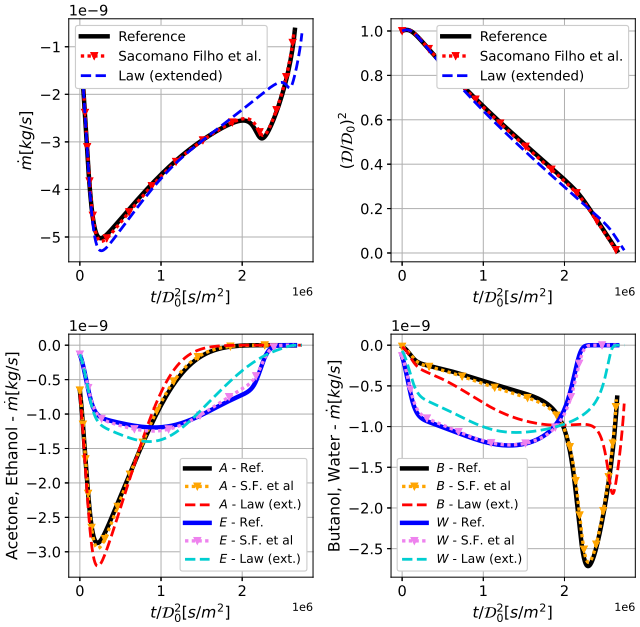

Figure 10: Acetone/ethanol/butanol/water (A/E/B/W) droplet with $\mathcal{D}_0 = 20\mu m$, $T_{d,0} = 300K$, $T^\infty = 1800K$, $U_{d,0} = 0m/s$, and $U^\infty = 0m/s$. The faraway state is composed of pure air. Results are displayed for the global mass transfer rate $\dot{m}$, the normalized diameter squared $(\mathcal{D}/\mathcal{D}_0)^2$ and individual mass transfer rates $\dot{m}_k$ for each species, versus a reduced time $t/\mathcal{D}_0^2$.

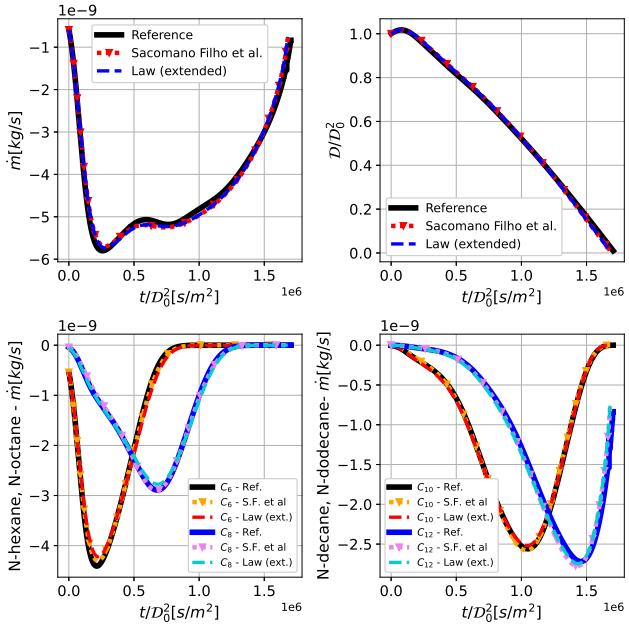

Figure 11: N-hexane/N-octane/N-decane/N-dodecane (Alk) droplet with $\mathcal{D}_0 = 20\mu m$, $T_{d,0} = 300K$, $T^\infty = 1800K$, $U_{d,0} = 0m/s$, and $U^\infty = 0m/s$. The faraway state is composed of pure air. Results are displayed for the global mass transfer rate $\dot{m}$, the normalized diameter squared $(\mathcal{D}/\mathcal{D}_0)^2$ and individual mass transfer rates $\dot{m}_k$ for each species, versus a reduced time $t/\mathcal{D}_0^2$.

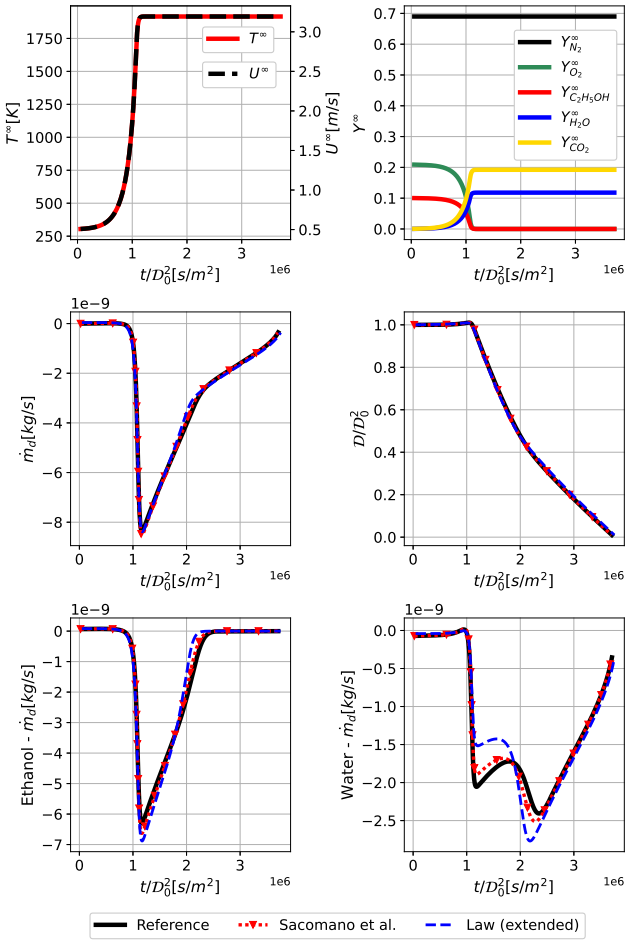

Figure 12: Ethanol/water (E/W) droplet with $\mathcal{D}_0 = 20\mu m$, $T_{d,0} = 300K$ and $U_{d,0} = 0.5m/s$ against a premixed laminar Ethanol stoichiometric flame. The surrounding gaseous temperature, composition, and velocity are embedded in the figure. Results are displayed for the global mass transfer rate $\dot{m}$, the normalized diameter squared $(\mathcal{D}/\mathcal{D}_0)^2$ and individual mass transfer rates $\dot{m}_k$ for each species, versus a reduced time $t/\mathcal{D}_0^2$.

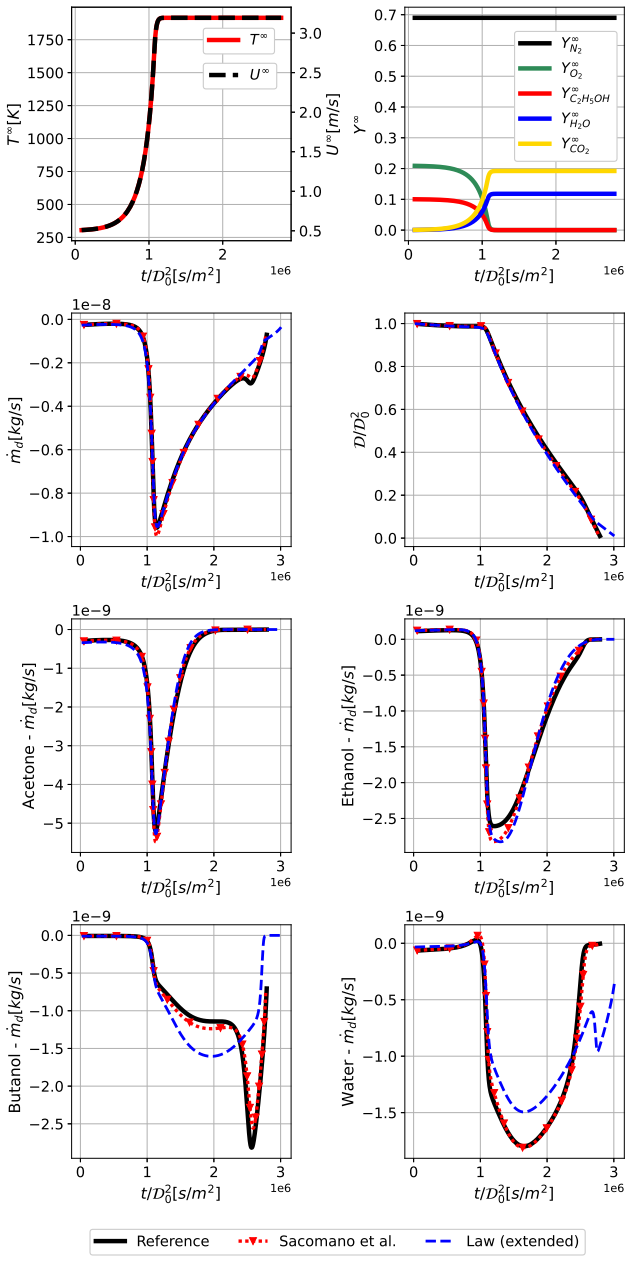

Figure 13: Acetone/ethanol/butanol/water (A/E/B/W) droplet with $\mathcal{D}_0 = 20\mu m$, $T_{d,0} = 300K$ and $U_{d,0} = 0.5m/s$ against a premixed laminar Ethanol stoichiometric flame. The surrounding gaseous temperature, composition, and velocity are embedded in the figure. Results are displayed for the global mass transfer rate $\dot{m}$, the normalized diameter squared $(\mathcal{D}/\mathcal{D}_0)^2$ and individual mass transfer rates $\dot{m}_k$ for each species, versus a reduced time $t/\mathcal{D}_0^2$.

Nomenclature

B_M	Spalding mass transfer number
$\bar{B}_M$	Average Spalding mass transfer number
$B_{M,k}$	Spalding mass transfer number of species k
B_T	Spalding heat transfer number
c	Molar density (mol/m^3)
$c_{p,k}$	Gaseous specific heat at constant pressure for species k ($J/(kg \cdot K)$)
$\mathcal{D}_0$	Droplet initial diameter (m)
$\bar{D}$	Average diffusion coefficient when assumed equal between all species (m^2/s)
D_k	Average multi-component diffusion coefficient between species k and the remainder of the multi-component mixture (m^2/s)
$D_{k,j}$	Binary diffusion coefficient between species k and j in a binary mixture (m^2/s)
$\tilde{D}_{k,j}$	Binary diffusion coefficient between species k and j in a multi-component mixture (m^2/s)
$D^T_{k,j}$	Thermal diffusion coefficient between species k and j ($kg/(m \cdot s)$)
F_M	Average correction factor to incorporate Stefan flow effects
$F_{M,k}$	Correction factor to incorporate Stefan flow effects for species k
$\mathbf{f}_k$	Volumetric forces field on species k (N)
m_d	Droplet mass (kg)
$\dot{m}$	Gaseous mass transfer rate (kg/s)
$\dot{m}_d$	Droplet mass transfer rate, $\dot{m}_d = -\dot{m}$ (kg/s)
$\dot{m}_k$	Mass transfer rate of species k (kg/s)
$\dot{n}_k$	Molar transfer rate of species k (mol/s)
Nu^*	Nusselt number with Stefan flow effects
$\mathbf{p}$	Pressure field (Pa)
$\dot{Q}$	Heat transfer rate (J/s)
r	Radial coordinate
R	Universal gas constant ($J/(mol \cdot K)$)
R_d	Droplet instantaneous radius (m)
Sh_0	Sherwood number in the absence of Stefan flow effects
$\bar{Sh}_0$	Average Sherwood number in the absence of Stefan flow effects
Sh^*	Sherwood number with Stefan flow effects
$\bar{Sh}^*$	Average Sherwood number with Stefan flow effects
$Sh_{k,0}$	Sherwood number of species k in the absence of Stefan flow effects
Sh^*_k	Sherwood number of species k with Stefan flow effects
t	Time (s)
T	Temperature (K)
$T_{d,0}$	Droplet initial temperature (K)
T^s	Temperature at the surface of the droplet (K)
T^∞	Temperature far away from the droplet (K)
$\mathbf{u}$	Velocity field (m/s)
$U_{d,0}$	Droplet initial velocity (m/s)
U^∞	Surrounding field velocity (m/s)
$\mathbf{v}^D_k$	Mass diffusion velocity of species k (m/s)
$\mathbf{v}^m_k$	Average molecular velocity of species k (m/s)
W_k	Molar weight of species k (kg/mol)
X_k	Molar fraction of species k
Y_k	Mass fraction of species k
$\bar{Y}_F$	Sum of mass fraction of all species that participate in phase-change
δ_M	Average mass boundary layer thickness (m)
$\delta_{M,k}$	Mass boundary layer thickness of species k(m)
ε_k	Fractional evaporation rate of species k, $\varepsilon_k = \dot{m}_k/\dot{m}$
λ	Thermal conductivity ($W/(m \cdot K)$)
ρ	Density (kg/m^3)
$\dot{\omega}_k$	Chemical reaction source term, species k ($kg/(m^3 \cdot s)$)